Translational buffering tunes gene expression in mouse and human

Authors: Shilpa Rao[1], Aden Y Le[1], Logan Persyn[1], Can Cenik[1]

[1] Department of Molecular Biosciences, University of Texas at Austin, Austin, TX 78712, USA

Keywords: Translational buffering, Ribosome occupancy, Translation efficiency, mRNA variation

Abstract: Translational buffering refers to the regulation of ribosome occupancy to offset the effects of transcriptional variation. Previous studies have primarily investigated translational buffering in yeast due to genetic variation or environmental stress. However, it remains unclear how widespread translational buffering is across mammalian genes in various cellular contexts. In this study, we uniformly analyzed 1515 matched ribosome profiling and RNA-seq datasets from human and mouse. This resource enabled us to assess translational buffering by comparative analysis of variation at ribosome occupancy and the RNA expression and by examining the relationship between mRNA abundance and translation efficiency. We found that translational buffering is partly conserved between human and mouse, with homologous genes showing a moderate cross-species correlation in mRNA–translation efficiency relationships and a strong enrichment of shared buffered genes, particularly those encoding ribosomal, RNA-binding, and proteasomal proteins. Although the identified buffered genes show association with some sequence features, these alone are insufficient to predict translational buffering, highlighting the importance of cellular context. Genes exhibiting translational buffering have lower variation in protein abundance in cancer cell lines as well as human and mouse tissues. We also observed that translationally buffered genes are more likely to be haploinsufficient and triplosensitive suggesting a demand for stringent dosage limits in these genes. We hypothesize two models of translational buffering, namely “differential accessibility model” and “translation initiation rate model” with our analysis suggesting that some transcripts conform to the former and others align with the latter. Our study explores the translational buffering potential of genes across diverse cellular conditions, elucidates the distinctive features of genes that exhibit this phenomenon, and provides insights into the possible mechanisms driving this effect.

Introduction:

mRNA variability arises from the inherent randomness of transcriptional events and in response to extrinsic fluctuations in the cellular environment. The randomness in transcription is driven by the stochastic nature of molecular interactions, whereas extrinsic noise reflects variation among cells in global factors such as metabolic state, signaling activity, cell cycle stage, and overall cell physiology [1–3]. In addition, genetic differences arising from aneuploidy, cell type diversity or those present within the natural population can further determine the amplitude of variation [4–7]. The effect of mRNA variation under these conditions is reflected at the protein levels for some genes. In other cases, however, it can be counteracted at the post-transcriptional level to minimize its effect on the protein abundance [2,4–9]. The mechanisms that can achieve this attenuation remain poorly characterized possibly involving excess protein degradation or translational buffering [4,6,10–15].

In this study, we define "translational buffering" as the post transcriptional mechanism wherein alterations in mRNA abundance is counteracted by changes in ribosome occupancy of transcripts. Early studies using allele-specific analyses of ribosome profiling and mRNA sequencing in yeast hybrids found that differences in mRNA abundance did not frequently lead to corresponding differences in ribosome occupancy [16,17]. More recent work profiled eight natural *S. cerevisiae* isolates using parallel RNA sequencing and ribosome profiling, and found that strain-to-strain transcriptional variation is buffered at the translational level [18]. While these studies focused on the impact of genetic differences on gene expression, translational buffering also underlies the cellular response to environmental stress. In yeast cells experiencing acute oxidative stress, aside from a small set of transcriptionally induced antioxidant genes, most mRNA expression changes were counteracted by opposite changes in ribosome occupancy resulting in negligible net protein change [19]. Similarly, translational buffering of certain genes have been reported in mammalian cells, specifically under estrogen receptor alpha depletion conditions [20]. Another comparative study that profiled both the transcriptome and translatome of three primary organs across five mammalian species and one bird observed buffering, characterized by reduced divergence at the translatome layer of especially essential and housekeeping genes [21]. Together, these studies of the impact of genetic variation, stress conditions and evolution suggest that cells often buffers or attenuates transcriptomic differences at the translation step, thereby stabilizing the proteome across different genotypes and environments.

Nonetheless, the prevalence of translational buffering among mammalian genes across different cellular contexts remains poorly characterized. Using matched measurements of

mRNA abundance and ribosome occupancy from RNA-seq and ribosome profiling experiments, we can assess two related but distinct types of relationships between mRNA abundance and ribosome occupancy (see [10,15] for discussion of analogous comparisons in the context of mRNA-protein abundance relationship). First, in a given condition, we can determine the effect of mRNA abundance on ribosome occupancy across transcripts. This is informative to understand gene specific differences in the efficiencies of translation. Modest correlation between mRNA abundance and ribosome occupancy levels and a higher correlation between ribosome occupancy and their corresponding protein levels [22] iterates the significance of ribosome occupancy determinants in understanding the steady state levels of different proteins in a given condition. Second, ribosome profiling with matched mRNA-seq enables exploration of the effect of mRNA variation of a particular gene on its ribosome occupancy across different experimental conditions.

In this study, we analyzed the effect of mRNA variation on ribosome occupancy across diverse cellular conditions by leveraging a repository called RiboBase, harboring 1,282 human and 995 mouse ribosome profiling data with matched RNA-seq experiments [23]. The vastly increased number of experimental samples provides much higher statistical power to detect genes that are translationally buffered. Our definition of translational buffering is based on the observation that some genes show minimal variation in the ribosome occupancy levels despite having varied mRNA abundance across hundreds of experiments. This implies a negative correlation between the translation efficiency (TE) and mRNA abundance of buffered genes. Overall, our study identifies the potential of genes to be translationally buffered and elucidates the possible mechanisms and rationale for this phenomenon.

Results:

Estimation of translation buffering potential of more than 8,000 genes.

To systematically identify genes that exhibit translational buffering, we analyzed how variation in mRNA abundance affects ribosome occupancy and TE in over 8,000 genes (Methods). We leveraged 2,277 matched ribosome profiling and RNA-seq datasets from 90 human and 82 mouse tissues and cell lines compiled in a comprehensive database (RiboBase)[23]. Using this resource, we calculated TE similarly to [23], with some modifications. We estimate TE using a compositional regression model [23], rather than the commonly applied approach of using a logarithmic ratio of ribosome occupancy to mRNA abundance. The ratio-based approach introduces spurious correlations between the resulting TE and the mRNA

abundance, which can confound interpretation [24,25]. In contrast to [23], we do not summarize TE by cell lines and instead use estimates from individual samples to capture a higher dynamic range of mRNA abundance which is essential for analysing translational buffering **(Sup. Table 1-4)**. Next, we implemented a geometric Bayesian-multiplicative imputation procedure that preserves compositional structure and relative proportions, yielding more reliable TE estimates. Lastly, we introduced an additional quality control filter to exclude samples displaying non-linear relationships between mRNA abundance and ribosome occupancy (Methods). Such non-linearities often result from cellular perturbations, such as genetic modifications or pharmacological interventions and render regression residuals unreliable estimates of TE (Methods). In total, we retained TE estimates for 8433 human and 8135 mouse candidate transcripts from 965 human and 550 mouse samples (1515 total), respectively **(Sup. Tables 5-6)**.

For most genes, ribosome occupancy scales linearly or near-linearly with mRNA abundance, hence TE is only weakly dependent on transcript abundance (**Fig 1A**). We reasoned that deviations from this pattern could be used to nominate genes exhibiting translation buffering. To identify such cases, we calculated pairwise correlations among TE, ribosome occupancy, and mRNA abundance across all human and mouse samples. The resulting wide distribution of correlation values suggests that mRNA variation differentially relates to TE and ribosome occupancy across genes **(Fig 1B-C**, **Sup. Fig 1 A-B)**. We used strong negative correlation between mRNA abundance and TE as a primary indicator of translational buffering. As expected, there was considerable overlap between the set of genes with lowest correlation between either mRNA-TE or mRNA-Ribosome occupancy (176 out of top 250).

As a second criterion, we identified genes with minimal changes in ribosome occupancy relative to variation in mRNA abundance. Our rationale is that if ribosome occupancy remains relatively constant despite substantial fluctuations in transcript abundance, this may indicate compensation at the level of translation. To quantify this, we calculated the median absolute deviation (MAD) for both ribosome occupancy and mRNA abundance across all samples in RiboBase **(Fig 1D-E)**. We then determined genes with low ribosome occupancy MAD relative to their mRNA MAD **(Fig 1F-G)**. Based on these two criteria, genes were ranked and categorized as “TB high” (top 250), “TB low” (next 250), and “Others” (remaining genes) **(Sup. Tables 7-8).** Example genes in each category from human and mouse are shown in **Fig 1H-M** and **Sup. Fig 1C- H**.

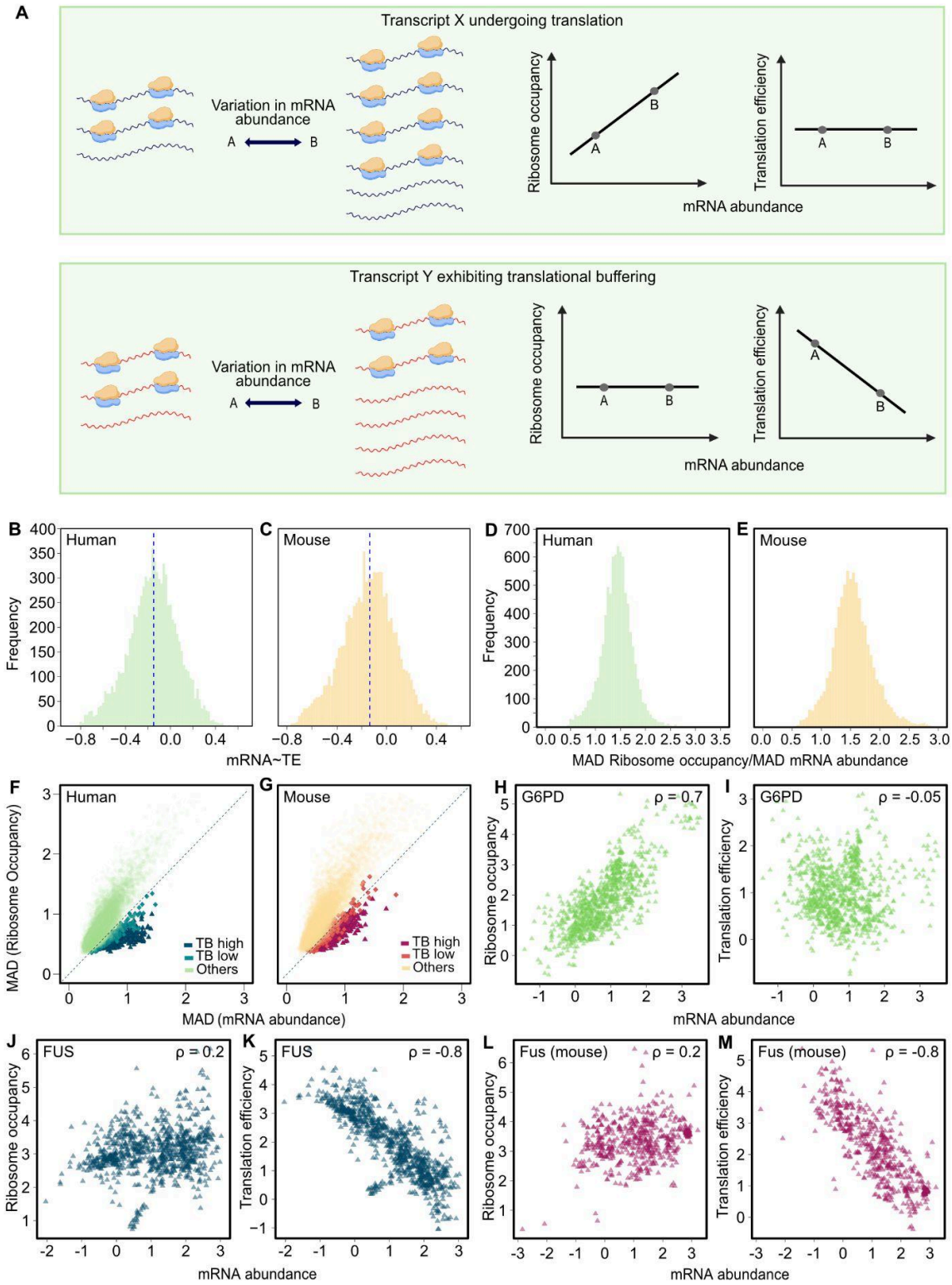
A
Transcript X undergoing translation
Variation in mRNA abundance
A
B
Ribosome occupancy
Translation efficiency
mRNA abundance
Transcript Y exhibiting translational buffering
B
Human
Frequency
mRNA~TE
C
Mouse
D
Human
MAD Ribosome occupancy/MAD mRNA abundance
E
Mouse
F
Human
MAD (Ribosome Occupancy)
MAD (mRNA abundance)
TB high
TB low
Others
G
Mouse
H
G6PD
ρ = 0.7
I
G6PD
ρ = -0.05
J
FUS
ρ = 0.2
K
FUS
ρ = -0.8
L
Fus (mouse)
ρ = 0.2
M
Fus (mouse)
ρ = -0.8

Fig 1: A. Schematic depiction of translational buffering: Transcript X shows linear relationship between mRNA abundance and ribosome occupancy resulting in no correlation between translation efficiency (TE) and mRNA abundance between condition A and B. Transcript Y shows no relationship between mRNA abundance and ribosome occupancy resulting in a negative correlation between translation efficiency and mRNA abundance between condition A and B. Hence transcript Y is considered to be translationally buffered. **B**. Distribution of Spearman correlation between mRNA abundance and translation efficiency calculated from ribosome profiling and matched RNA-seq of 965 human samples for 8433 human genes. The blue dashed line indicates the median of the correlation **C**. Distribution of Spearman correlation (ρ) between mRNA abundance and translation efficiency calculated from ribosome profiling and matched RNA-seq of 550 mouse samples of 8135 mouse genes. **D**. Distribution of the ratio of median absolute deviation (MAD) of ribosome occupancy vs MAD of mRNA abundance for human genes. **E**. for mouse genes. **F.** Scatter plot of MAD of mRNA abundance and MAD of ribosome occupancy for all genes in RiboBase for humans **G.** for mouse. Each point indicates a gene and the color depicts their buffering category. The dashed line indicates the line of equivalence**. H. & I.** Relationship between mRNA abundance and ribosome occupancy or translation efficiency of human non-buffered gene; G6PD, **J & K.** human buffered gene; FUS, **L & M.** mouse buffered gene; Fus. Each point is the information from a ribosome profiling and matched RNA-seq experiment for the given gene. All values are clr normalised (see methods)

Conservation of translational buffering across species and its determinants

We hypothesized that if translational buffering is functionally important or inherently associated with specific transcript features, it would be conserved across species. To test this, we assessed the relationship between the mRNA-TE Spearman correlation values for homologous genes in human and mouse. We found a moderate correlation (~0.6), indicating that the relationship between mRNA abundance and TE is partially conserved between these two species **(Fig 2A)**.

Notably, 126 genes were shared among the top 250 translationally buffered genes (**Sup. Table 9;** Fisher's exact test odds ratio 83.4; p-value < $2.2*10^{-16}$). These genes include ribosomal proteins (n=55), RNA binding proteins (n=32), chromatin binding/transcriptional regulators (n=11), proteasomal complex proteins (n=7), genes involved in the electron transport chain complexes (n=6) and 15 others **(Fig 2B)**. This distribution of genes suggests that genes encoding for components of macromolecular complexes may preferentially be enriched for translational buffering **(Sup. Fig 2 A&B)**.

The conservation of translational buffering suggests that intrinsic transcript properties might contribute to this phenomenon. Hence, we compared various features, and found that the translationally buffered gene set had lower median CDS length and 3`-UTR length in human and mouse (Wilcoxon rank-sum test p-value < $1.0 *10^{-3}$ comparing TB high and TB others; **Fig 2C-D)**. Our analysis also reveals that highly ranked genes show associations with particular features, indicating an underlying hierarchy in translational buffering potential **(Sup. Fig 3A-B)**.

Further, GC content of 5`-UTR was analysed for in both human and mouse with the later species showing a significantly lower 5`-UTR GC content potentially indicative of a propensity for increased secondary structures in the buffered set (Wilcoxon rank-sum test p-value ($1.2*10^{-7}$ of TB high vs. TB others and mouse) **(Sup. Fig 3C-D, Sup. Tables 10-11)**.

To understand if codon usage patterns are associated with translational buffering, we next analyzed codon properties across buffered and non-buffered human gene sets. The codon adaptation index quantifies how closely a gene's codon usage aligns with that of highly expressed genes [26]. Genes in the buffered gene set had a higher codon adaptation index than the non-buffered set. Specifically, 28.4% of TB high genes, 14% of TB low genes and 9.3% of genes in the other category fall within the top decile (>90th percentile) of codon adaptation index **(Sup. Fig 4A, Sup. Table 12)**.

Growing evidence suggests that translation initiation rates can be modulated by elongation speed, which is itself influenced by codon usage [27,28]. Consequently, the codon composition of a transcript may determine its translational tunability. Consistently buffered gene candidates (both TB high and low) have a higher proportion of certain codons including that of lysine (AAG), proline (CCT, CCC, CCA), alanine (GCT), and glutamine **(Fig 2E, Sup. Fig 4B, Sup. Table 13)**. Next, we analyzed the enrichment of certain codons associated with mRNA stability in HEK293T cells [29]. We observed a significant correlation between codon stabilization coefficient and the difference in codon frequency between buffered and non-buffered genes for both TB high (ρ =0.3, p-value= 0.02) and TB low (ρ =0.3, p-value= 0.01) categories, indicating that buffered genes are slightly enriched for codons associated with higher mRNA stability.

Given the observation with higher codon adaptation index and stability coefficients, we next analyzed if translationally buffered genes had higher average transcript abundance. We observed that the TB high transcripts had a slightly higher median mRNA abundance across all samples compared to genes with TB low and non-buffered gene sets (Wilcoxon rank-sum test p-value $6.9 * 10^{-58}$ for TB high vs. others and $1.2 * 10^{-15}$ for TB low vs. others; **Fig 2F, Sup. Table 7)**. Approximately, 52.8 % of TB high genes, 21.6% of TB low genes and 8.3% of genes in the other category fall within the top decile (>90th percentile) of median RNA expression. A similar trend was evident in mouse samples which predominantly represent primary tissue samples (Wilcoxon rank-sum test p-value $1.7*10^{-51}$ for TB high vs. others and $6.4*10^{-23}$ for TB low vs. others; **Fig 2G, Sup. Table 8)**. Although genes with the highest MAD values are not translationally buffered, we observed that non-buffered genes in both humans and mice exhibit lower variation in mRNA abundance across samples. These findings suggest that genes with

either very high or very low MAD values are less likely to be translationally buffered **(Sup. Fig 3E-F)**. Collectively our analysis suggests that translationally buffered genes differ in intrinsic features, such as length, GC content, codon usage bias and expression levels.

To test if these sequence features are sufficient to determine translational buffering, we trained regression and classification models on features derived from the mRNA sequence and experimental data (Methods). These features were previously shown to be predictive of TE [30] and mRNA stability [31]. Specifically, we used light gradient-boosting machine (LGBM) models. The objective of the regression task was to predict the mRNA-TE Spearman correlation. An LGBM regression model trained only on sequence features achieved an r^2 of 0.24 (**Fig 2H**). For the binary classification task, TB high and TB low genes were assigned the positive label and all other genes, the negative label. We trained models on three different sets of features: i) a model trained only on sequence features, ii) a model trained only on experimental features, and iii) a model trained on both combined feature sets (Methods). The models scored an average precision of 0.34, 0.49, and 0.53, respectively, while randomly assigning labels based on class balance achieves an average precision of 0.06 (**Fig 2I**). The classification model trained on sequence features attributed high importance to many of the same features found to be enriched in TB genes discussed earlier (e.g. the codons GGU (Gly) and AAG (Lys), and CDS length; **Fig 2J**) .The enrichment of these codons or lower CDS length is associated with lower mRNA–TE correlation (negative spearman correlation) and hence a lower TB rank (rho $\propto$ TB rank). However, the modest performance observed suggests that the mRNA sequence alone is insufficient to predict translational buffering. The models that incorporate the experimental features outperform the sequence only model, further supporting the idea that cellular context is important in predicting translational buffering (**Fig 2I**).

To investigate potential trans-acting determinants of translational buffering, we focused on 1,394 human RBPs as classified by [32]. Specifically, we examined correlations between the RNA expression of each RBP and the TE of all other genes across samples. This analysis revealed that the expression levels of many RBPs are significantly enriched for either positive or negative correlations with the TE of buffered genes (**Sup. Fig 5**). In particular, we note that RNA expression of many buffered RBPs is enriched for negative correlations with the TE of other buffered transcripts. These results suggest that, rather than considering translational buffering in isolation for each transcript, buffering effects may be coordinated at the translational level and influenced by shared trans-acting factors such as RBPs. Network-based approaches have been valuable for RNA co-expression and are only now being applied to TE covariation [33]. However, the correlative nature of these analyses limits causal inference. For example,

although many ribosomal proteins appear to influence the buffering of other ribosomal proteins, they themselves may be regulated by a non-ribosomal RBP—so the apparent effects could reflect upstream regulatory influences. Together, the analysis suggests that both cis and trans acting factors might contribute to translational buffering of genes.

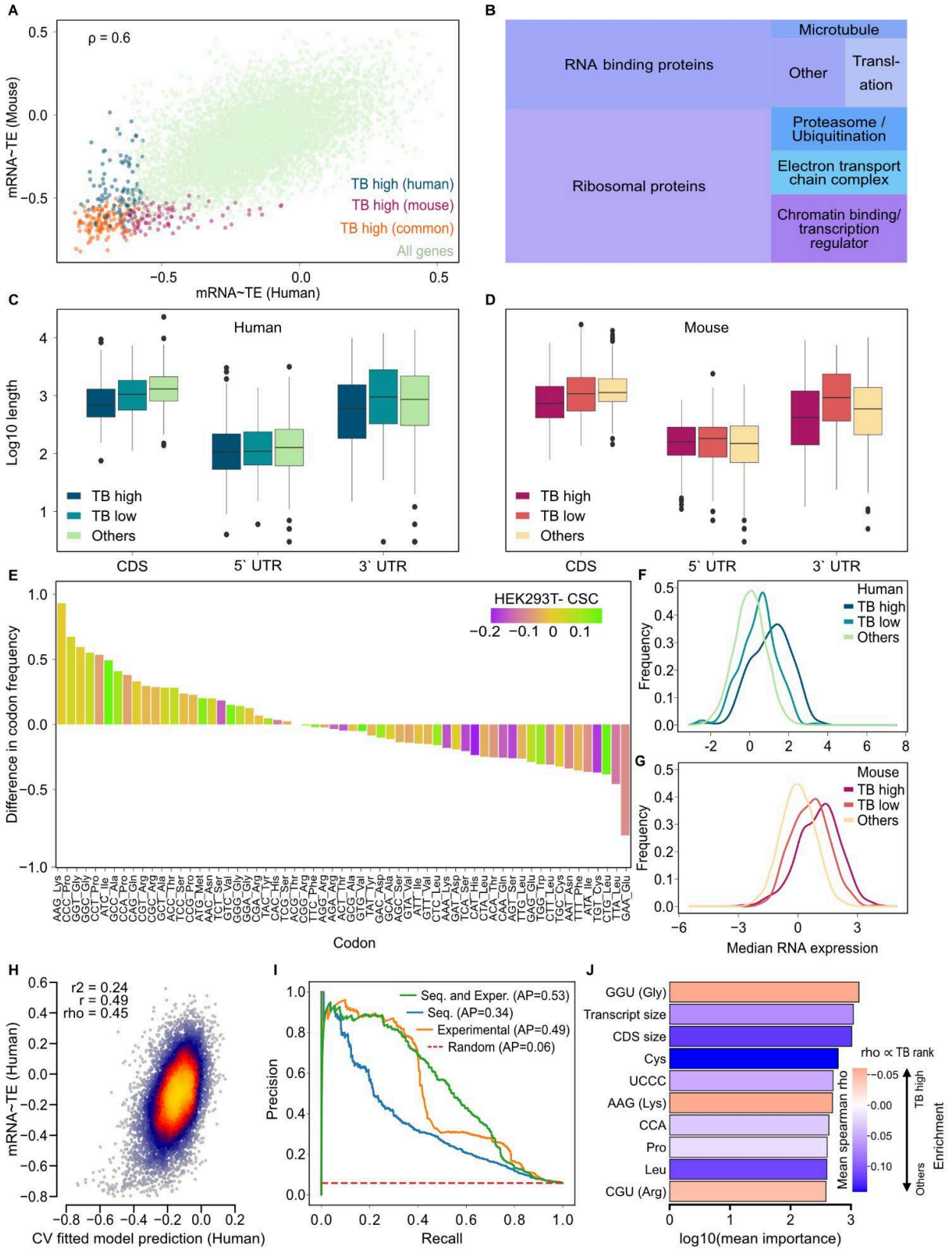
A
ρ = 0.6
mRNA~TE (Mouse)
mRNA~TE (Human)
TB high (human)
TB high (mouse)
TB high (common)
All genes
B
RNA binding proteins
Ribosomal proteins
Microtubule
Other
Transl-ation
Proteasome / Ubiquitination
Electron transport chain complex
Chromatin binding/ transcription regulator
C
Human
Log10 length
TB high
TB low
Others
CDS
5` UTR
3` UTR
D
Mouse
TB high
TB low
Others
CDS
5` UTR
3` UTR
E
HEK293T- CSC
Difference in codon frequency
Codon
F
Human
TB high
TB low
Others
Frequency
G
Mouse
TB high
TB low
Others
Frequency
Median RNA expression
H
r2 = 0.24
r = 0.49
rho = 0.45
mRNA~TE (Human)
CV fitted model prediction (Human)
I
Seq. and Exper. (AP=0.53)
Seq. (AP=0.34)
Experimental (AP=0.49)
Random (AP=0.06)
Precision
Recall
J
GGU (Gly)
Transcript size
CDS size
Cys
UCCC
AAG (Lys)
CCA
Pro
Leu
CGU (Arg)
rho ∝ TB rank
Mean spearman rho
TB high
Others
Enrichment
log10(mean importance)

Fig 2: A. Scatter plot showing the relationship between mRNA abundance ~ translation efficiency (TE) correlations between human and mouse (Spearman correlation coefficient = 0.6, p-value < 2.2e-16). **B.** Treemap showing the categories of genes that overlap between human and mouse top 250 (TB high) identified translationally buffered genes. Box plot showing the length of CDS, 5`-UTR and 3`-UTR of the three categories (TB high, low and others) of **C.** human genes (TB high n=250, TB low n= 245; Others n=495) **D.** mouse genes (TB high n=250, TB low n= 250; Others n=500) The y axis indicates $\log_{10}$ values. Gene in TB others category were selected after a matching procedure (See Methods). **E.** Bar plot showing the difference in codon frequency between "high" and non-buffered genes The bars are colored according to the codon stabilization coefficient obtained from [29]. Density plot of median mRNA abundance across all samples in all three categories in **F.** human (TB high n=250, TB low n= 250; TB others n=7933) and **G.** mouse (TB high n=250, TB low n= 250; TB others n=7635). **H.** Scatter plot comparing predicted and observed human mRNA-TE Spearman correlation across 10 CV folds. The r^2, Pearson (r), and Spearman (rho) correlation coefficients between predicted and observed are also shown. **I.** Precision-recall curves of LGBM models trained on three different sets of features: Sequence, Experimental, and both sets combined (Seq. and Exper.). Average precision (AP) for each model is shown along with the performance of randomly predicting class labels. **J.** The top 10 most important features determined by the sequence LGBM classification model (Methods). The bar color corresponds to the Spearman correlation between the feature and each gene's translational buffering candidate rank. Note that a feature with a negative Spearman correlation indicates an enrichment in genes with lower mRNA–TE correlation. n refers to the number of genes.

<u>Translational buffering offsets the impact of mRNA variation on protein abundance.</u>

Translational buffering could be expected to reduce fluctuations in their protein amounts due to changes in mRNA abundance **(Fig 3A)**. To evaluate this, we compared the protein abundance variation using mass spectrometry data from 949 human cancer cell lines [34], 32 human primary tissues [35] and 41 mouse tissues [36]. Consistent with the expectation, buffered gene sets (TB high and low) had lower median absolute deviation in protein abundance compared to all non-buffered genes across all three datasets: in cancer cell lines (Wilcoxon rank-sum test p-value $5 * 10^{-39}$ for TB high vs. others and $3 * 10^{-23}$ for TB low vs. others) **(Fig 3B; Sup. Fig 6A)**, in human **(Fig 3C; Sup Fig 6B)** and mouse tissues **(Fig 3D ;Sup Fig 6C).** To ensure that this reduced protein abundance variability was not simply explained by mRNA abundance differences, we selected non-buffered gene sets that are matched to buffered categories (both high and low) in terms of their mRNA MAD (Methods). Even after matching on variance in mRNA abundance, we observed a similarly lower deviation in protein abundance of buffered genes in human cancer cells (Wilcoxon rank-sum test p-value $2 * 10^{-29}$ for TB high vs. others and $4.5 * 10^{-19}$ for TB low vs. others) and mouse tissue samples (Wilcoxon rank-sum test p-value $8.4 * 10^{-26}$ for TB high vs. others and $3 * 10^{-8}$ for TB low vs. others). However, the

difference in MAD (protein abundance) became statistically insignificant for human tissue samples **(Sup. Fig 6D-F)** as translationally buffered genes exhibited lower deviation in mRNA abundance compared to non-buffered genes in this particular dataset. These results indicate that translational buffering contributes to reduced protein variability across conditions, beyond what can be explained by mRNA variation alone.

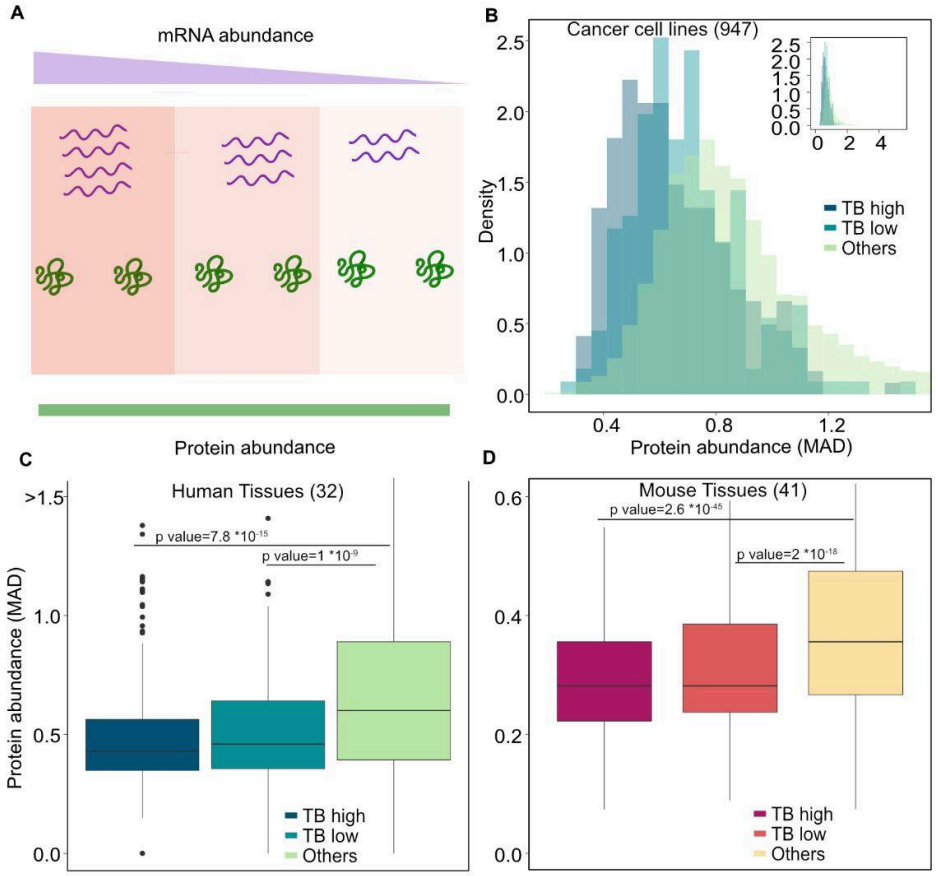

Fig 3: A. Schematic of the mRNA protein relationship in translational buffering **B.** Normalized histogram showing the MAD of protein abundance of genes in the three categories from human cancer cell lines (TB high n=221, TB low n= 202; Others n= 7954) **B.** Boxplot showing the MAD of protein abundance of genes in the three categories from **C.** human primary tissue (TB high n=233, TB low n= 227; Others n= 12167) and **D.** mouse tissues (TB high n=189 TB low n= 199; Others n= 6113). n refers to the number of genes

<u>Translational buffered genes are more likely to exhibit haploinsufficiency and triplosensitivity</u>

Translational buffering dampens the impact of transcript abundance fluctuations on protein output and may serve as a mechanism to stabilize protein abundance across conditions. This property suggests the possibility that translational buffering preferentially occurs in

dosage-sensitive genes as an evolved mechanism to maintain proteomic homeostasis. Alternatively, if buffering mitigates the consequences of reduction of transcript abundance, it may render genes more tolerant to dosage perturbations, predicting a depletion of haploinsufficient genes among the buffered set. To evaluate these competing hypotheses, we examined the correspondence between translational buffering and gene-level dosage sensitivity using population-based metrics **(Fig 4A)**. Specifically, we first used the probability of loss of function intolerance (pLI score) as provided by the gNOMAD database. We found that buffered gene sets had higher pLI scores (median for TB high= 0.86, TB low= 0.76 and TB others= 0.0018), indicating increased likelihood of haploinsufficiency **(Fig 4B)**. A chi-squared test revealed a highly significant difference in the distribution of genes across score ranges among the three categories (χ^2 = 519.5, df = 18, $p < 2.2\times 10^{-16}$), indicating that gene distributions differed substantially between them.

To further investigate the relationship between translational buffering and dosage sensitivity, we analyzed a second dataset that estimates haploinsufficiency and triplosensitivity for autosomal genes [37]. Genes in the translationally buffered sets had higher pHaplo scores (median for TB high= 0.802, TB mid= 0.697 and TB others= 0.48; $\chi^2(18) = 114.8$, p value= 4×10^{-16}, **Sup. Fig 7A**) and pTriplo scores (median for TB high= 0.638, TB low= 0.785 and TB others= 0.43, $\chi^2(18) = 151.3$, p-value< 2.2×10^{-16}) compared to non-buffered genes (**Fig 4C)**. These findings suggest that translationally buffered genes are more likely to exhibit dosage sensitivity and may have evolved for more stringent control of protein abundance.

The observed propensity for haploinsufficiency and triplosensitivity implies that translational buffering alone is insufficient to compensate for the large (~50%) perturbation at the transcript level. Instead, translational buffering can likely counterbalance only minor fluctuations in mRNA abundance. This interpretation is also consistent with depletion of genes with high variability at the mRNA level among those that exhibit translational buffering **(Fig 1F)**.

To further test this interpretation, we analyzed if experimental manipulation via siRNA or CRISPR knockdown could be compensated at the ribosome occupancy level (Methods). These perturbations, like haploinsufficiency and triplosensitivity, involve substantial reductions in transcript abundance and thus represent major perturbations beyond the range of typical physiological variation. For both TB high and TB low gene sets, experimental mRNA knockdown led to concordant reductions in ribosome occupancy proportional to the observed decrease in mRNA abundance **(Fig 4D)**. However, the limited number of experiments with direct perturbation of buffered genes limit the generalizability of this observation.

Finally, we analyze the effect of natural variation at the level of RNA on ribosome occupancy levels [6] across lymphoblastoid cell lines from a diverse group of individuals. In contrast to the experimentally induced knockdowns or dosage sensitivity, this setting captures endogenous, inter-individual variability in transcript abundance under physiological conditions. As before, we selected genes with matched mRNA MAD across the three sets (TB high, low and others; **Fig 4E, Sup. Table 14**). Despite matched transcript-level variation, TB high genes exhibited significantly lower variability in ribosome occupancy compared to the non-buffered group (Wilcoxon rank-sum test p-value=$3.9*10^{-4}$ and $4.8*10^{-3}$ for TB high or low vs. others, respectively). Taken together, these findings suggest that translational buffering likely functions as a homeostatic mechanism in response to physiological variation, but is insufficient to mitigate the effects of large-scale transcript perturbations.

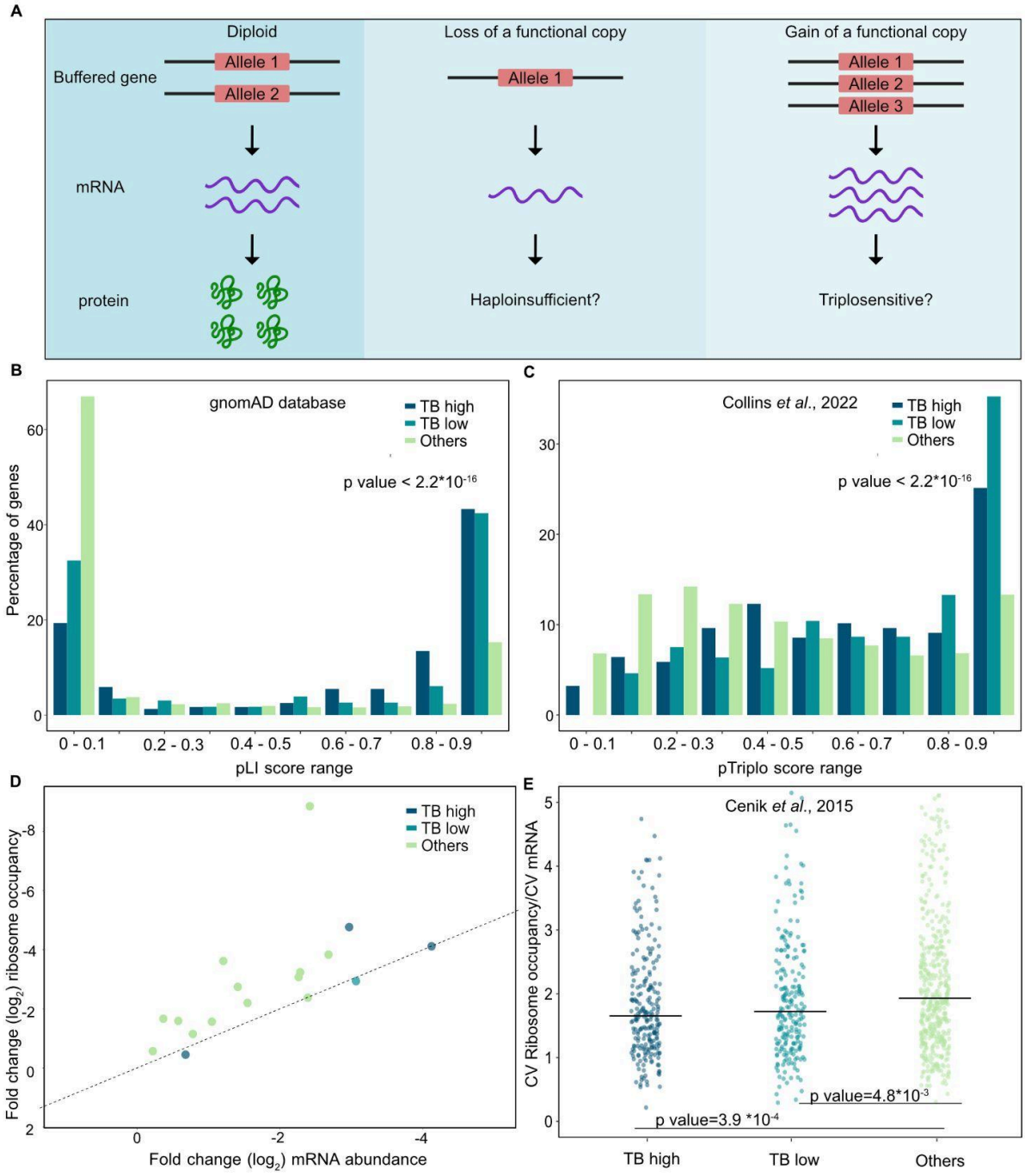

Fig 4: A. Schematic for the hypothesis whether the buffered gene sets are intolerant or tolerant towards dosage perturbations **B.** The gNOMAD database provides a pLI score (Probability of Loss of Function Intolerance) that predicts how likely a gene is able to tolerate loss-of-function mutations. Bar plot shows that buffered gene sets have a higher median pLI score (TB high n=238, TB mid n= 231; TB others; n= 18728) **C.** Collins et al. 2022 predicts the triplosensitivity for all autosomal genes referred to as pTriplo score. The bar plot shows a higher median pTriplo score (TB high n=187, TB mid n= 173; TB others; n= 11128) than the non-buffered set. n refers

to the number of genes **D.** Plot showing the log2 fold change in mRNA abundance and ribosome occupancy in samples involving CRISPRi/siRNA knockdown of buffered and non-buffered genes from RiboBase. The color indicates the buffering category. Each dot represents a specific gene.Only genes that show significant change in mRNA abundance and Ribosome occupancy (p value <0.05) are plotted. **E.** Plot showing the ratio of Ribosome occupancy (CV) and mRNA abundance (CV) of genes analysed from lymphoblastoid cell lines. The genes in the "other" category were selected by a matching approach (Methods). The horizontal bar indicates the median of the ratio was lower in buffered genes than non-buffered genes (TB high n=235, TB mid n= 222; TB others; n= 457).

The association of translationally buffered genes with the translational machinery varies in response to changes in mRNA abundance

We next explored the potential mechanisms that may give rise to translational buffering. Specifically, we considered two non-mutually exclusive models by which mRNA abundance might be decoupled from ribosome occupancy. In the first, the "differential transcript accessibility model", mRNA abundance determines the fraction of transcripts that are accessible to the translational pool. In this scenario, an increase in mRNA abundance would be accompanied by a proportionally smaller increase in the fraction of transcripts entering the translating pool for buffered genes, compared to non-buffered genes. In the second, the "initiation rate model", the rate of translation initiation per transcript scales inversely with mRNA abundance. Under this model, as mRNA abundance increases, translation initiation on each transcript is reduced, thereby lowering the number of ribosomes per transcript. However, this mechanism allows a proportional increase in transcripts entering the translational pool for buffered genes, similar to non-buffered genes **(Fig 5A)**.

To evaluate the relative contributions of these models, we performed sequencing of both total and translating RNA fractions in HEK293T cells (Methods), leveraging variation in mRNA abundance across replicates. We considered genes that were in the top half in terms of mRNA variation as measured by coefficient of variation, and excluded genes with poor linearity between total and translating RNA (Methods). We then calculated the slope of the linear relationship between total and translating mRNA abundance across replicates. We observed a broad range of slopes (from < –1 to ~1), where a slope of ~0 would indicate minimal changes in the translating pool despite variation in total mRNA, and a slope near 1 would reflect a proportional increase in translation. Negative slopes, observed in some cases, likely reflect measurement errors and technical artifacts (e.g., ribosome dissociation during ultracentrifugation).

We found that genes in the “TB high” category exhibited significantly higher slopes compared to non-buffered genes (**Fig 5B, Sup. Table 15;** Wilcoxon rank-sum test p-value 5 $*10^{-7}$ for TB high vs. others; 1.26 $*10^{-1}$ for TB low vs. others). Yet, consistent with our earlier observation from RiboBase, these genes vary less at the ribosome occupancy levels (lower CV) compared to non-buffered gene set (**Fig 5C;** Wilcoxon rank-sum test p-value 1.2 $*10^{-3}$ for TB high vs. others; 7.5 $*10^{-1}$ for TB low vs. others), indicating that increased access to the translational pool does not translate into proportional increases in ribosome loading. A similar trend was observed when genes from non-buffered set were selected to match the mRNA CV of the buffered gene set, confirming that buffered genes have a higher tendency to enter the translational pool despite comparable mRNA variability (Wilcoxon rank-sum test p-value 1.2 $*10^{-5}$ for TB high vs. others; 1.3 $*10^{-1}$ for TB low vs. others), while having lower ribosome occupancy variation (Wilcoxon rank-sum test p-value 1.8 $*10^{-2}$ for TB high vs. others; 8.7 $*10^{-1}$ for TB low vs. others **Sup. Fig 8A-B)**.

One caveat of this approach is the assumption that transcripts recovered following ultracentrifugation are exclusively associated with ribosomes. However, some transcripts may be bound to large ribonucleoprotein complexes that co-sediment with ribosome-associated mRNAs. Given this possibility, the slope for buffered transcripts could also be higher if their initiation rate does not change but the excess of buffered transcripts are bound by large ribonucleoprotein complexes.

To further examine the relationship between transcript abundance and engagement with the translational machinery, we employed an alternative analytical approach. We compared the relative abundance of transcripts in the translating pool versus the total RNA fraction between buffered and non-buffered gene sets. Consistent with the previous analyses, genes in the TB high category had a relatively higher fraction of genes in the translational pool compared to non-buffered genes as measured by calculating the $\log_2$ fold change between the translating pool and total RNA (Methods) (Wilcoxon rank-sum test p-value 7.8 $*10^{-8}$ for TB high vs. others; **Fig 5D, Sup. Table 16)**. This enrichment could potentially be biased by differences in mRNA abundance. Even after matching for transcript abundance, buffered genes retained a significantly higher association with the translational pool (Wilcoxon rank-sum test p-value 1.3 $*10^{-29}$ for TB high vs. others; 7.3 $*10^{-29}$ for TB low vs. others; **Sup. Fig 8C**) indicating that mRNA abundance does not alone account for their preferential engagement with the translation machinery. Taken together, these findings suggest that both the initiation rate models and the differential transcript accessibility may contribute to translational buffering. Further studies will

be required to clarify the relative contributions of these mechanisms and delineate their molecular mechanisms.

Finally, we analysed mRNA stability of the three categories. We compared the half life of buffered vs non-buffered transcripts [38]. Translationally buffered genes had longer mRNA half-life compared to non-buffered genes (median: TB high; 625 minutes, TB low; 352.5 and TB others; 195 minutes) (Wilcoxon rank-sum test p-value 2 $*10^{-60}$ for TB high vs. others; 2.1 $*10^{-25}$ for TB low vs. others; **Fig 5E**). This observation is consistent with genes in the TB high category being enriched for codons associated with higher stability (**Fig 2E**). To gain insight into the kinetics of half life of transcripts in each of the subcellular locations, we leveraged TimeLap-seq data [38]. This analysis suggested that the transcripts from the TB high category spend more time in the cytoplasm (half life in cytoplasm; median: TB high; 135 min, TB low; 105 min, others; 75 min) however are quicker in loading to the polysome fraction (half life in untranslated cytoplasm (median: TB high; 2.3 min, TB low; 5.4 min others; 10 min; **Fig 5F**)**.** Translationally buffered transcripts also seemed to be exported more slowly from the nucleus than non-buffered transcripts (half life in cytoplasm; median: TB high; 135 min, TB low; 106 min, others; 80 min). On comparing the subcellular half life of transcripts similar in their whole cell half life (Methods), the buffered transcripts (TB high) have a higher half life in both cytoplasm (half life in cytoplasm; median: TB high; 135 min, TB low; 105 min, others; 75 min) and nucleus (half life in nucleus; median: TB high; 135 min, TB low; 105 min, others; 80 min) **(Sup. Fig 8D)**. Overall, these observations indicate that buffered transcripts differ from non-buffered sets in their RNA flow dynamics and have a higher possibility of association probably for a longer time with the translational machinery than the non-buffered transcripts.

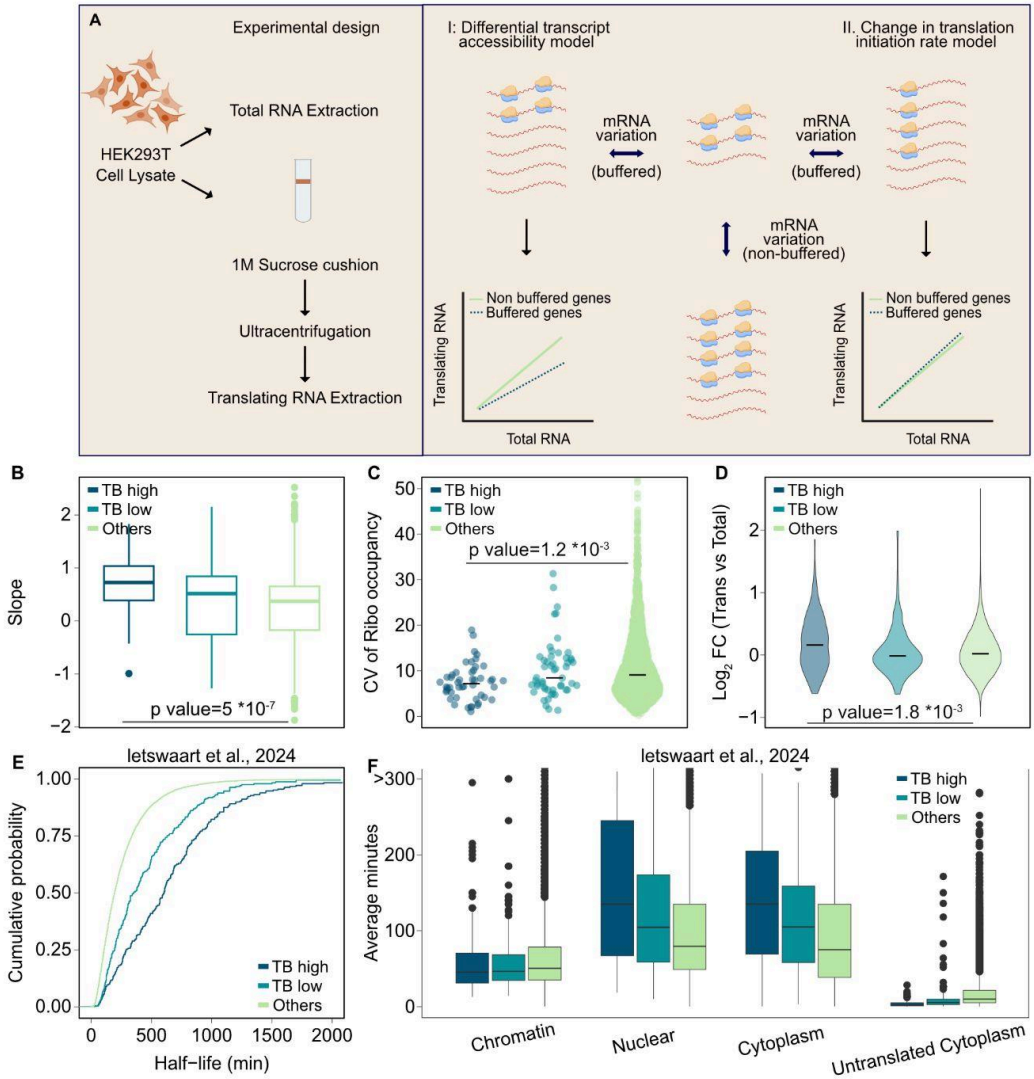

Fig 5: A. Schematic of experimental design to analyze the possible mechanism of translational buffering. **B.** Box plot showing the slope between translational RNA and total RNA (See Methods) for the buffered and non-buffered gene set (TB high n=48,TB low n= 52; TB others n=2157). The slope was higher in the buffered gene set which indicates that as the total mRNA abundance changes, a considerable fraction of buffered transcripts enter the translating pool as the non-buffered gene set. **C.** Sina plot showing the CV of ribosome occupancy levels of the three gene sets from the ribosome profiling experiment carried out in parallel to the RNA-seq of total and translating RNA (See Methods) (TB high n=48, TB low n= 52; TB others; n=2153). **D.** Violin plot showing the $\log_2$ fold change between the translational mRNA and total mRNA of all genes present in three categories (TB high n=250, TB low n= 250; TB others n=11889). **E.** Empirical cumulative distribution function (ECDF) plot showing the distribution of half life of mRNA for the three categories of gene sets (TB high n=249, TB low n= 246; TB others n=17670) **F.** Box plot showing the half life measurements of the three categories of gene sets (TB high n=249, TB low n= 246; TB others n=17670) in different compartments including the

chromatin, nucleus, untranslated cytoplasm and the cytoplasm. The half life measurements of mRNA were obtained from [38]. n refers the number of genes

Discussion

Ribosome occupancy of certain transcripts remains relatively unchanged, even when their mRNA levels vary across conditions. This phenomenon has been referred to as "post-transcriptional buffering" in several yeast studies [17–19] and as "translational buffering" in others [20,39]. Across these studies, differences in species evaluated, statistical methods and definitions of buffering have resulted in conflicting interpretations [10,15,25,40].

To systematically characterize translational buffering at the transcriptome scale and to evaluate this phenomenon across different conditions, we leveraged a compendium (RiboBase) of more than a thousand ribosome profiling datasets with matched RNA-seq measurements [23]. This resource enabled us to quantify how variation in mRNA abundance across samples influences ribosome occupancy and TE. The breadth of experimental conditions, encompassing a range of human cell lines and mouse primary tissues, provided robust statistical power to detect translational buffering across diverse cellular contexts. Though we relied on a subjective threshold for defining genes as "TB high or low", we emphasize that genes span a continuum of translational buffering potential, with certain genes demonstrating more stringent control (TB high and low) over ribosome occupancy levels than others (TB others).

Estimating the translational efficiency from ribosome profiling and matched RNA-seq data remains an area of debate. The method we used to calculate TE is based on a compositional regression model [23], rather than the commonly applied approach of using a logarithmic ratio of ribosome occupancy to mRNA abundance. The ratio-based approach introduces spurious correlations between the resulting TE and the mRNA abundance, which can confound interpretation [24,25]. Several methods that have been developed previously for measuring changes in TE [41–43]. These are designed to be used in experimental designs where there is a treatment or manipulation that is assayed along with controls. While these methods are highly valuable in assessing differential TE, they are unable to accommodate the type of meta-analyses described in our study. The combination of a large sample size across diverse conditions independently evaluated in two species, along with our TE calculation method, offers a distinct advantage for studying translational buffering and expanding its interpretation across species.

Our analyses revealed substantial overlap in translationally buffered genes between human and mouse, despite the differing sources of the underlying datasets. While human samples were predominantly derived from cell lines, mouse samples originated largely from

tissues. This concordance across species suggests that translational buffering may be conserved for a subset of genes. Many of these genes encode components of multiprotein complexes, such as ribosomes, the electron transport chain, and the proteasome, all of which have previously been shown to exhibit translational buffering in yeast as well [17–19]. However, the set of translationally buffered genes can vary depending on cellular or environmental context, as with observations in natural isolates and different growth conditions [18].

In both human and mouse datasets, translationally buffered genes are typically highly expressed and often encode dosage-sensitive complexes, including the ribosome. The change in absolute transcript abundance for these highly expressed genes in response to intrinsic or extrinsic noise would be substantial compared to lowly expressed genes. This likely necessitates more stringent regulation. Hence, translational buffering may serve as a compensatory mechanism, limiting protein production from these abundant transcripts to ensure that protein synthesis remains within physiological limits.

In addition to their expression levels, transcripts also exhibit varying degrees of fluctuation across samples. Certain buffered genes show a higher stringency in their mRNA variation. For example, we observed that constitutively expressed genes like ribosomal genes and GAPDH exhibit modest variation in mRNA levels across conditions, consistent with findings in yeast [18]. Recent studies have also reported sub-Poissonian mRNA distributions for some constitutively expressed genes in yeast [44]. In contrast, other buffered gene candidates, such as FUS, display significant variation in mRNA levels across samples, suggesting less stringent transcriptional control. This may require a more robust buffering mechanism. However, whether these two cases differ in their buffering mechanisms remains to be determined. Additionally, it would be counterproductive to allow high variation in transcript levels only to later balance it at the translational level. While this could be due to stochastic fluctuations in mRNA, it is interesting to speculate that mRNA variability in certain genes may sequester regulatory molecules such as RNA binding proteins.

Many transcripts in the TB high category encode ribosomal proteins characterized by the presence of TOP motifs whose TE is known to be co-regulated in response to environmental cues mainly through the mTOR pathway [45]. Our analysis suggests that their TE is possibly altered in relation to fluctuations in transcript levels to potentially minimize variation in protein abundance. Recent reports suggest that TOP transcripts are known to be associated with sub-polysomal fractions and represent translationally repressed transcripts [46,47]. Such a repression may facilitate translational buffering in some transcripts.

Although we observed associations between specific sequence features and translational buffering, these are unlikely to be the sole determinants. This is supported by our machine learning model, which shows that sequence alone is insufficient to accurately predict genes exhibiting translational buffering. Furthermore, the model indicates that features within the coding sequence are more informative than those in the untranslated regions. The limited predictive power of sequence features alone suggests that cellular context likely plays a significant role in determining the translational buffering capacity. This is in contrast to translation efficiency itself which can be much more accurately predicted solely from mRNA sequence [30]

Beyond delineating the determinants of translational buffering, our study elucidates the adaptive value of this phenomenon. Earlier studies with a Drosophila brain tumor model suggested that fold change in protein abundance of genes involved in energy metabolism, transcription and translation have lower correlation with fold changes at mRNA levels (ρ= 0.23, ρ= 0.16, ρ= 0.45 respectively) than other complexes [48]. Other studies using aneuploidy cell lines indicated that though the mRNA expression correlates to the increased chromosome copy numbers, approximately a quarter of the proteins are less abundant than expected and more similar to their disomic context [8]. Our analysis suggests that regulation of ribosome occupancy by translational buffering could be one of the strategies adopted by the cells to achieve lower variation at protein level. Another rationale for some genes to exhibit translational buffering could be that cells could tune expression of genes regulated by the same transcription factors, thus allowing some targets but not others to ultimately end up with higher or lower protein levels.

The mechanistic basis of translational buffering remains incompletely understood. Recent work has shown that upstream open reading frames can buffer main ORF by inducing ribosome stalling, particularly through terminal diproline motifs under conditions of limited ribosome availability [49]. Our RNA-seq experiments of translating versus total RNA fractions provides evidence supporting the feasibility of two models: differential transcript accessibility to the translational machinery and modulation of translation initiation rate particularly in response to changes in mRNA abundance. The accessibility model is supported by analyses of transcript half-lives in nuclear and cytoplasmic compartments, which suggest that transcript availability to ribosomes may be regulated at the level of subcellular localization. In contrast, the fast loading of buffered transcripts on the polysomes also argues for the initiation rate modulation model. Since the half-life measurements reflect steady-state levels, investigating how mRNA variation

influences the spatial and temporal dynamics of transcripts could provide valuable insights into the mechanisms underlying translational buffering.

While this study expands our understanding of translational buffering, it has several important limitations. Firstly, our study is limited to genes that are robustly expressed in most samples thereby missing information on lowly or cell-type specifically expressed genes. Genes that are possibly translationally buffered in a particular cellular-context or tissue specific manner would escape our identification criteria. Further, our analysis relies on steady-state measurements of RNA abundance and ribosome occupancy, which may fail to capture dynamic or transient regulatory mechanisms that contribute to translational buffering. Next, most of the reported analyses are correlative in nature, therefore experimental manipulation of mRNA variability to analyse the effect on ribosome occupancy/TE might be needed. A potential drawback in understanding the models of translational buffering in response to natural variation in mRNA abundance is distinguishing true signal from technical noise. This challenge, coupled with a low replicate number (four), complicates the interpretation of slopes and the prediction of hypothesized models. Incomplete discrimination between mechanistic models, could potentially be due to insufficient molecular details. For instance, it remains unclear what specific molecular mechanisms are capable of sensing mRNA abundance variability and subsequently modulating translation initiation or accessibility. Clarifying this connection is crucial for distinguishing between models of translational buffering. We also note that ribosome occupancy is not always a reliable proxy for protein output, as additional factors such as translation elongation rates, ribosome stalling, and co-translational degradation can significantly influence the efficiency and outcome of protein synthesis.

Despite these caveats our study fills a gap in knowledge regarding translational buffering of genes in humans and mouse. Other model organisms such as *C.elegans* (nematodes), Drosophila, zebrafish have orders of magnitude less data making it difficult to assess translational buffering with high confidence. However, as more matched transcriptomic and translatomic datasets become available in other model organisms, extending this analysis will provide a broader perspective particularly in determining whether translational buffering is intrinsically encoded or primarily driven by cellular context. The availability of these datasets will also make it feasible to analyze translational buffering at the interspecies level. For example, many of the mitochondrial proteins were suggested to be translationally buffered under specific genetic backgrounds in *C.elegans* [50]. Hence, we speculate that this phenomenon may be conserved beyond mammalian genomes. Finally, complementary approaches such as live-cell imaging of translation at the single-transcript level under variable mRNA conditions could yield

mechanistic insights beyond what bulk analyses allow. Overall, our work expands the catalog of buffered genes, reveals their evolutionary conservation, highlights their potential functional constraints (e.g., dosage sensitivity), and offers a conceptual and computational framework for studying translational buffering in broader biological settings.

Methods:

Calculation of translational efficiency:

The method for calculating translation efficiency (TE) is adapted from [23], with some modifications. In this study, TE is calculated for each gene for individual samples in RiboBase rather than summarized at the cell line level as in [23]. For this, matched RNA-seq (PCR-deduplicated) and ribosome profiling read counts (non-deduplicated and winsorised) for 19,736 genes in 1,078 human and 21,569 genes in 846 mouse experiments were used **(Sup. Tables 1-4)**. The method of obtaining the RPF and RNA-seq read counts are described in [23]. We determined genes which have <1 count per million in more than 20% of the samples. In addition, we identified transcripts that lack a poly-A tail have artifactually "low" RNA -seq counts in experiments that rely on oligo-dT selection for library preparation, though their ribosome occupancy reads are well captured [6]. The corresponding raw read counts of all these transcripts were then collapsed and assigned to a "dummy gene". This was necessary because these genes, though part of the composition in the sample, were excluded from downstream analyses given their low expression across the compendium. In total, the dummy gene captures read counts corresponding to 10,859 genes. A small number of samples wherein the "dummy gene" contributed to more than 70% of the total counts were removed from analysis, reducing the number of experiments to ~1000.

A particular challenge in compositional data analysis is the handling of missing values . In this study, we used a geometric bayesian multiplicative imputation method from the R package zCompositions[51]. This function by default removes any samples which have more than 80% missing values in the sample (therefore removed 2 more samples). Genes with imputed values were used for conversion to their centred log ratio (clr) values. To calculate the TE, clr-normalized counts were converted to isometric log ratios. These values were used to generate a line of best fit between the two parameters and the residuals were defined as TE for each gene in a given sample. Samples which had R^2 less than 0.2 were removed as the residuals calculated for these samples could be unreliable. After these calculations, mRNA abundance, translational efficiency and ribosome occupancy values of 8,433 human genes from 965 samples and 8,135 mouse genes from 550 samples were retained for further analyses.

Assignment of translational buffering scores:

For each gene, Spearman correlation between mRNA abundance and either ribosome occupancy or TE was calculated across samples separately for human or mouse. Similarly, the

median absolute deviation (MAD) was computed for mRNA abundance and ribosome occupancy for each gene and the ratio of MAD for ribosome occupancy to that of mRNA abundance was calculated. We then ranked genes based on two metrics: (i) mRNA-TE correlation (with the most negative correlation ranked highest) (ii) MAD ratio (with lower ratio ranked higher). We then summed the ranks from both metrics and genes were re-ranked, with lower sums corresponding to higher final ranks.The top 250 genes were categorised as “TB high”, the next 250 “TB low” and the remaining genes as “Others”. To assess across species conservation, Spearman correlation was also computed between the mRNA-TE correlations of human and mouse orthologs and genes were annotated according to their respective translational buffering categories.

Gene ontology enrichment analysis:

Lists of TB high genes in human or mouse were analyzed using the enrichGO() function, with the organism-specific annotation database (org.Hs.eg.db for human or org.Mm.eg.db for mouse) as reference using clusterProfiler R package [52]. Gene identifiers were supplied as gene symbols, and all genes in the current study were used as the background universe. Enrichment was carried out for Biological Process, with significance assessed by the hypergeometric test. P-values were adjusted for multiple testing using the Benjamini–Hochberg method, and terms with an adjusted p-value < 0.05 were considered significant. To reduce redundancy among highly overlapping GO terms, results were post-processed with the simplify() function in clusterProfiler, which merges semantically similar terms. Visualization of the non-redundant enriched GO terms was performed using dot plots (dotplot()) showing the top terms ranked by adjusted p-value.

Sequence feature analysis:

Transcript region lengths were extracted from the APPRIS annotations using custom shell scripts. Corresponding nucleotide sequences were retrieved with bedtools v2.29.1 [53] and nucleotide content was computed using the Bioconductor Biostrings package v2.54.0 [54]. For both humans and mouse, the log10-transformed lengths of coding sequence, 5`UTR and 3`UTR length and GC content for each region were calculated for all genes.

To control for confounding sequence features, non-buffered genes (Others) were matched to the buffered genes based on either CDS length (for comparing UTR lengths) or UTR lengths (for comparing CDS lengths) using the MatchIT package (nearest neighbor method) [55]. Similarly,

for GC content comparisons, non-buffered genes were matched either on UTR GC content (for CDS GC content comparison) or on CDS GC content (for UTR GC content comparisons). Statistical differences between gene groups across sequence features were assessed using the Wilcoxon rank-sum test.

To analyze codon bias, codon frequencies were calculated for each human gene using custom R scripts and the BioString package [54]. Median mRNA abundance was computed across samples for each gene and the top fifth percentile of genes by expression was used to define the highly expressed set. The codon adaptation index was calculated using the cubar package [56]. Codon frequencies were computed for each buffering category and the difference in frequency between buffered (TB high & low) and non-buffered set (TB others) was calculated for each codon. To assess if the codon usage differences relate to transcript stability, the codon stabilization coefficient (CSE) obtained from [29] was compared to codon frequency difference using Pearson correlation.

Sequence based predictive modeling of translational buffering:

The sequence features used in the machine learning tasks were: i) the length, nucleotide composition, and {2-6}-mer frequencies across the 5`-UTR, CDS, 3`-UTR, and full transcript; ii) codon and amino acid usage; iii) wobble base composition; iv) the nucleotides at the -3, -2, -1, +4, and +5 Kozak positions; v) frequencies of dicodons that affect TE in yeast [57]; and vi) multiple secondary structure measures. The sequence features were computed with the same methods used previously [30]. The experimental features include various measures such as the number CLIP-seq and RIP-seq peaks for different RBPs [31]. LGBM models (lightgbm v3.2.1) [58] were trained with 10-fold cross validation. In the classification task, 20% of the training data for each fold was held as a validation set to calibrate the classifier. The default hyperparameters for the LGBM model were used except with the importance type set to “gain”. Feature importance was measured as the sum total information gain across all LGBM tree splits using that feature, averaged across all training folds.

RNA binding protein (RBP) correlation analysis:

To explore potential trans-acting determinants of translational buffering, we focused on 1,394 human RBPs as classified by [32]. We examined correlations between the RNA expression of each RBP and the TE of other genes across samples. P-values were corrected using the Bonferroni procedure, and Pearson correlations greater than 0.5 or less than -0.5 that met the p-value cutoff were considered significant for each RBP-gene pair. Subsequently, for each RBP,

we performed Fisher's exact test to evaluate whether significant correlations were enriched among buffered versus non-buffered genes. The Bonferroni procedure was also applied to determine the threshold for the odds ratio.

Proteomics data and analyses:
Protein abundance from 949 human cell lines [34], 32 human primary tissues [35] and 41 mouse tissues [36] were used to evaluate the effect of translational buffering on protein abundance variability. For each dataset, MAD of protein abundance was calculated across samples for each gene. To control for differences in transcript expression, non-buffered genes (TB others) were matched to buffered genes based on MAD of mRNA abundance using the nearest neighbor method implemented in the MatchIT package [55]. Differences in protein abundance variability between buffered and non-buffered gene sets were assessed using the Wilcoxon rank-sum test.

Dosage sensitivity among translationally buffered genes:
The gNOMAD database was used to retrieve the pLI score of all genes [59] followed by calculating the percentage of genes in each pLI score range. A second dataset providing predictions of haploinsufficiency (pHaplo score) and triplosensitivity (pTriplo score) for all autosomal genes [37] was used to assess the distribution of these scores across buffered and non-buffered gene sets. Comparisons were made to evaluate whether translationally buffered genes are enriched for dosage-sensitive characteristics. Differences between distributions were assessed using Pearson's chi-squared test of independence.

Differential expression analysis of knockdown experiments:
Ribosome profiling experiments and matched RNA-seq involving siRNA/CRISPRi-mediated knockdown of genes categorized as *TB-high*, *TB-low*, or *others* were retrieved from the RiboBase database[23]. For each experiment, the RNA-seq and ribosome profiling counts were normalized using the TMM normalization [60]. Transcript specific dispersion estimates were calculated and differentially expressed genes in each study were identified using edgeR [61].

Lymphoblastoid cell line data analysis:
To assess the impact of natural variation in mRNA levels on ribosome occupancy, we analyzed lymphoblastoid cell lines from genetically diverse individuals using data from Cenik et al [6].

Matched RNA-seq and ribosome profiling count files were obtained from GEO (accession: GSE65912). Only samples with both RNA and ribosome occupancy data were included in downstream analyses. For each gene, the coefficient of variation (CV) was calculated separately for mRNA abundance and ribosome occupancy across individuals. The ratio of CV for ribosome occupancy to CV for mRNA abundance was then computed in R. To generate a background gene set (*TB others*), genes were matched to the *TB-high* and *TB-low* groups based on their mRNA CVs using the nearest-neighbor method in the MatchIt package [55].

Cell culture:
HEK293T cell lines were obtained from ATCC. HEK293T cell lines were maintained in Dulbecco's modified Eagle's media (DMEM, GIBCO) supplemented with 10% Fetal Bovine Serum (FBS, GeminiBio) and 1% Penicillin and Streptomycin (GIBCO, Life Technologies) at 37°C in 5% CO_2 atmosphere. Cell lines were tested for mycoplasma contamination every 6 months and were consistently found negative.

Translating and total RNA isolation and sequencing:
Four replicates of ~8 X10^6 HEK293T cells were plated in 150 cm2 plates (see Supplementary text). After ~18 h, cells were washed and then scraped with ice cold PBS, followed by centrifugation at 300g for 5 min. 600 µl Lysis buffer (20 mM Tris, 150 mM NaCl, 5 mM MgCl2, 1mM DTT, Triton and 100 µg/ml of cycloheximide) was added to the cell pellet followed by incubation on ice for 10 min and the lysate was clarified by centrifugation at 1300g for 10 min at 4°C. The cleared lysate (50 µl) was directly used for total RNA extraction by adding 700 µl of Trizol (Zymo Research). 200 µl of the lysate (translating RNA) along with 20 µl of the Ribonucleoside Vanadyl Complex was layered on the 1M sucrose cushion and subjected to ultracentrifugation at 38,000 rpm for 2.5 h at 4°C to isolate the translating RNA. The remaining 350 µl was used for ribosome profiling. The pellet was dislodged in 700 µl of Qiazol and stored -80°C until use the next day. Total RNA and translating RNA was extracted using Zymo RNA miniprep kit as per manufacturer's protocol (Zymo Research). The concentration was estimated using nanodrop and the integrity of the extracted RNA was determined by 2100 Bioanalyzer (RNA 6000 Pico Kit, Agilient). 1µg of the extracted RNA was used for poly(A) selection using NEBNext poly(A) mRNA magnetic isolation kit (NEB, E7490S). This was followed by library preparation using NEBNext Ultra II RNA library prep kit for Illumina (NEB, E7770S) as per the manufacturer's protocol using 7 PCR cycles. The quality and concentration of the libraries

formed were determined by Bioanalyzer (High sensitivity DNA assay kit, Agilient). Equimolar amounts of the libraries were pooled and sequencing on NovaSeqX Plus (2X150 paired end).

Ribosome profiling:

For ribosome profiling, 350 µl of lysate was digested with 5 µl of RNase (Ambion) for 30 min at room temperature, layered on 1M sucrose solution followed by ultracentrifugation. The RNA was isolated using miRNeasy Mini kit and size-selected by running 1 µg of each sample in a 15% polyacrylamide TBE-UREA gel. 26–34 nt RNA fragments were excised, RNA fragments were extracted and precipitated as described in [62]. Ribosome profiling libraries were prepared using the D-Plex Small RNA-Seq Kit (Diagenode) as previously described [62]. The cDNA was amplified for eleven cycles. Each library was cleaned with AMPure XP beads and eluted with 30 µL of RNase-free water. To completely remove the primer-dimers, size-selection was done using a 12% polyacrylamide gel followed by excision of the fragment (~200bp). The DNA was extracted by overnight incubation in a buffer (10 mM magnesium acetate tetrahydrate, 0.5 M ammonium acetate, 1 mM EDTA (pH 8.0) at room temperature followed by ethanol precipitation (-20°C, overnight) to recover the size selected libraries. The resulting libraries were analyzed with the Agilent High Sensitivity DNA Kit (Agilent). Each library was mixed in equimolar proportion for sequencing with the NovaSeqX Plus (2X150 paired end).

Analysis of translating RNA/total RNA and ribosome profiling data:

Ribosome profiling and the matched RNA-seq experiments (4 replicates each) were processed using RiboFlow [63] as before [62] and leveraged RiboGraph for data visualization [64]. Genes with >10 counts per million in more than 6 samples were retained. We then fitted a linear regression line using lm function in R and determined the slope between the translating and total RNA. Genes with an R^2 value less than the median, indicating a non-linear relationship between translating RNA and total RNA, were removed from. In addition, genes with low variability between replicates (i.e CV of RNA between replicates, < median CV) were also filtered out. After applying these, 2,257 genes were analysed. To ensure that differences in slope and the variation in ribosome occupancy were not due to differences in mRNA variation, genes in the non-buffered gene set were matched to the buffered gene set based on mRNA CV using the nearest-neighbor method in the MatchIt package [55]. To analyze the differential engagement of buffered and non-buffered gene sets with the translating pool, differential analysis between the translating and total RNA was performed using edgeR [61]. To ensure that resulting log2 fold change between the translating pool and total RNA, is not contributed by

differences in mRNA abundance, genes in the non-buffered set were matched to the buffered gene set based on mRNA abundance (cpm) using the nearest-neighbor method in the MatchIt package [55].

Subcellular mRNA half life analysis:

mRNA half-life data were obtained from [38]. For each gene, we calculated the average mRNA half-life by taking the mean of replicate values across the chromatin, nuclear, cytoplasmic, and untranslated cytoplasmic fractions, along with the whole-cell mRNA half-life. This average was used as a representative measure of mRNA half life across subcellular compartments.

Supplementary Figures:

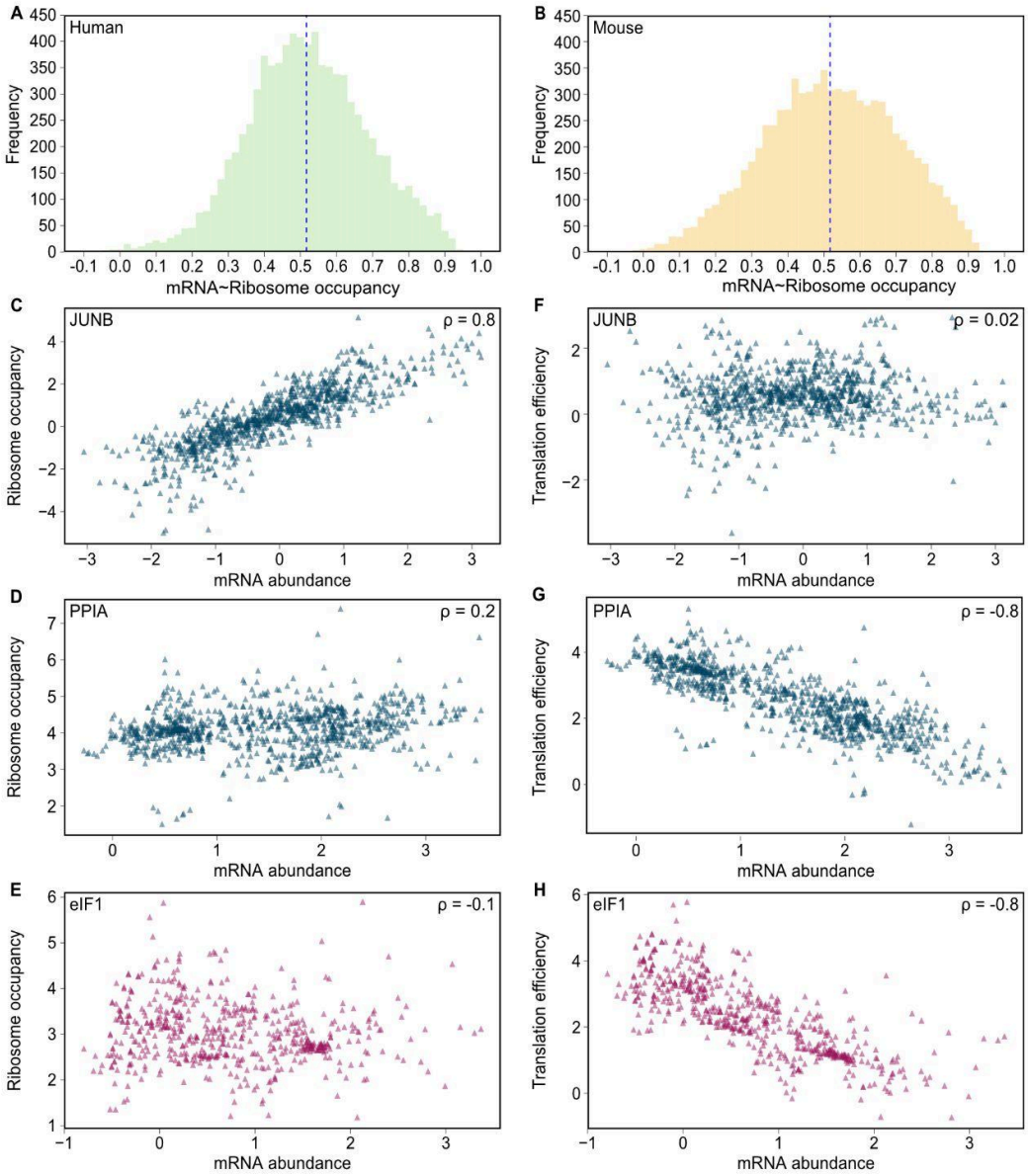

Sup. Fig 1: A. Spearman correlation between mRNA abundance and ribosome occupancy calculated from ribosome profiling and matched RNA-seq of 965 human samples for 8433 human genes **B**. Spearman correlation between mRNA abundance and ribosome occupancy calculated from ribosome profiling and matched RNA-seq of 550 mouse samples for 8135 mouse genes. Relationship between mRNA abundance and ribosome occupancy of a **C.** human non-buffered gene; JUNB **D.** human buffered gene; PPIA, **E.** mouse buffered gene; eIF1. Relationship between mRNA abundance and translation efficiency of a **F.** human non-buffered gene; JUNB, **G.** human buffered gene; PPIA, **H.** mouse buffered gene; eIF1. Each point is the information from a ribosome profiling and matched RNA-seq experiment for the given gene.

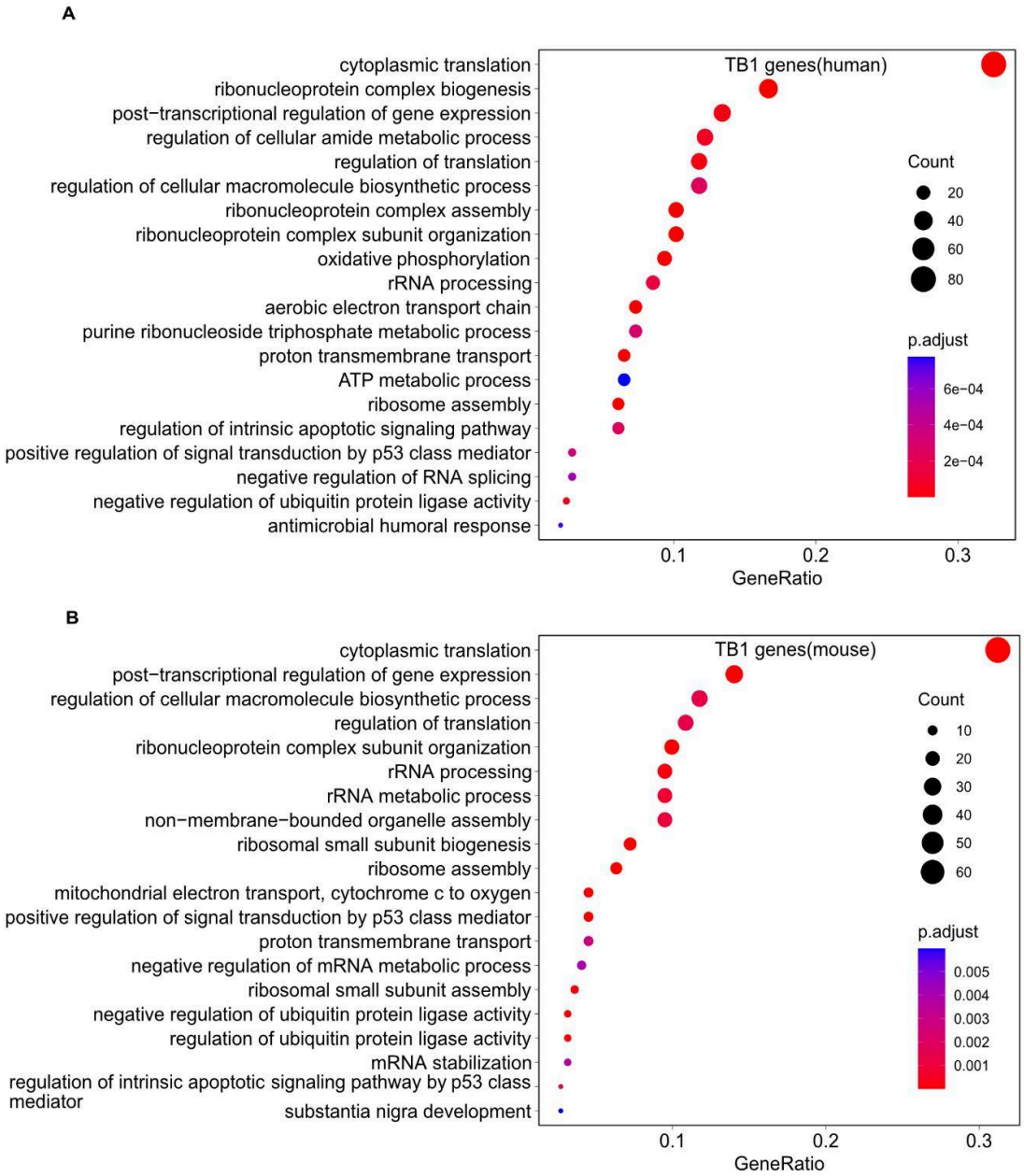

Sup. Fig 2 Gene Ontology (GO) enrichment analysis of the TB high gene set, performed with the clusterProfiler R package. Enriched GO Biological Process terms are shown after redundancy reduction. Each dot represents a GO term, with dot size indicating the number of genes associated with the term and color reflecting the adjusted p-value (Benjamini–Hochberg correction). Only the top non-redundant terms are displayed.

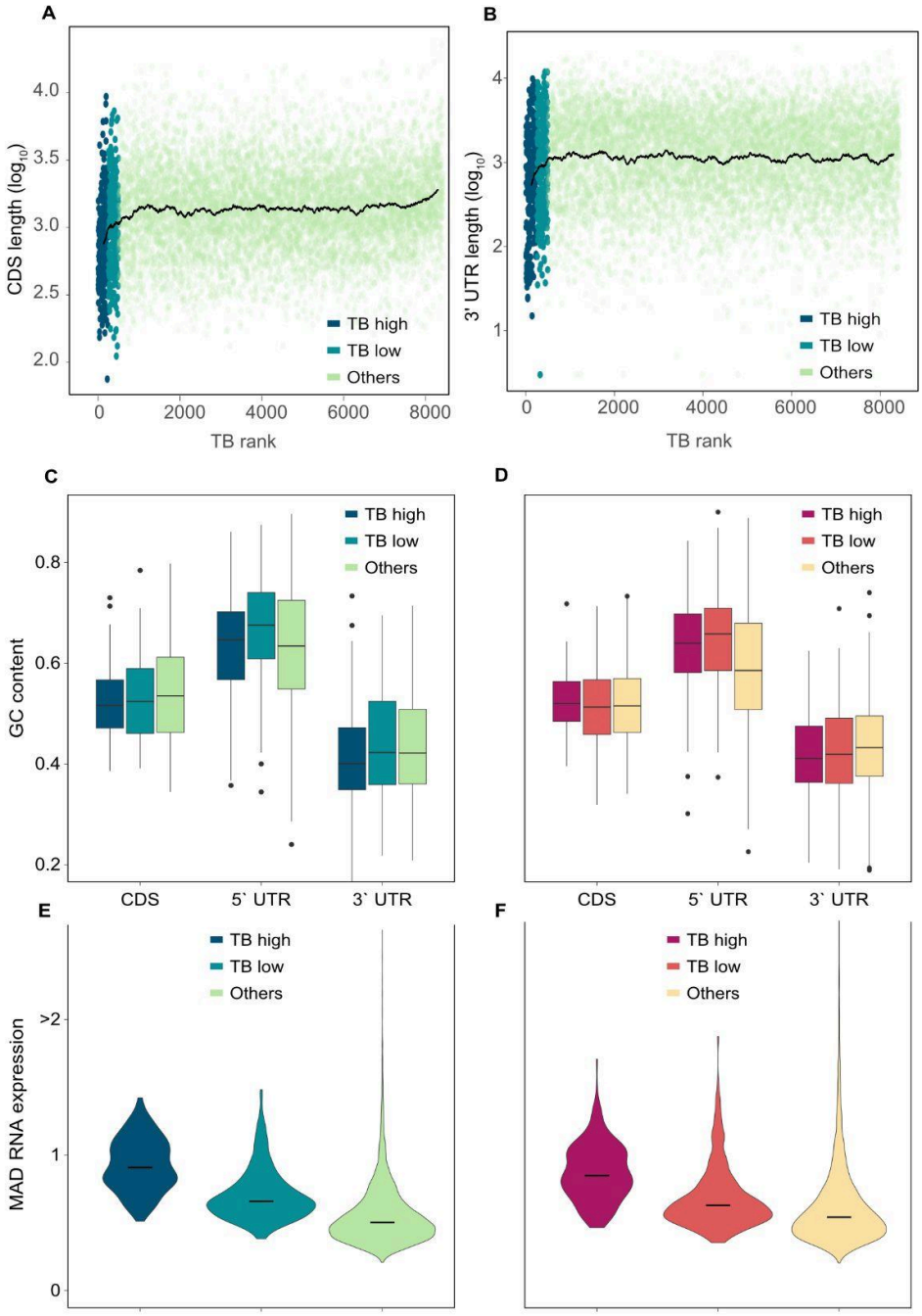

Sup. Fig 3. Scatter plot showing the relation between rank and **A**. CDS length and **B.** 3' UTR length. A moving average of CDS or 3' length was calculated using a centered 250-gene sliding window and is shown as the black line. Box plot showing the GC content of CDS, 5`-UTR and 3`-UTR of the three categories (TB high, low and others) of **C.** human genes (TB high; n=250, TB low; n= 245; others; n=495) **D.** mouse genes (TB high; n=250, TB low; n= 250; others; n=500) The y axis indicates GC content. Gene in the "other" category were selected after a matching approach (See Methods). Violin plot showing the median absolute deviation of mRNA

abundance of genes in all three categories in **E.** human (TB high; n=250, TB low; n= 250; others; n=7933) **E.** mouse (TB high; n=250, TB low; n= 250; others; n=7635) .n refers the number of genes

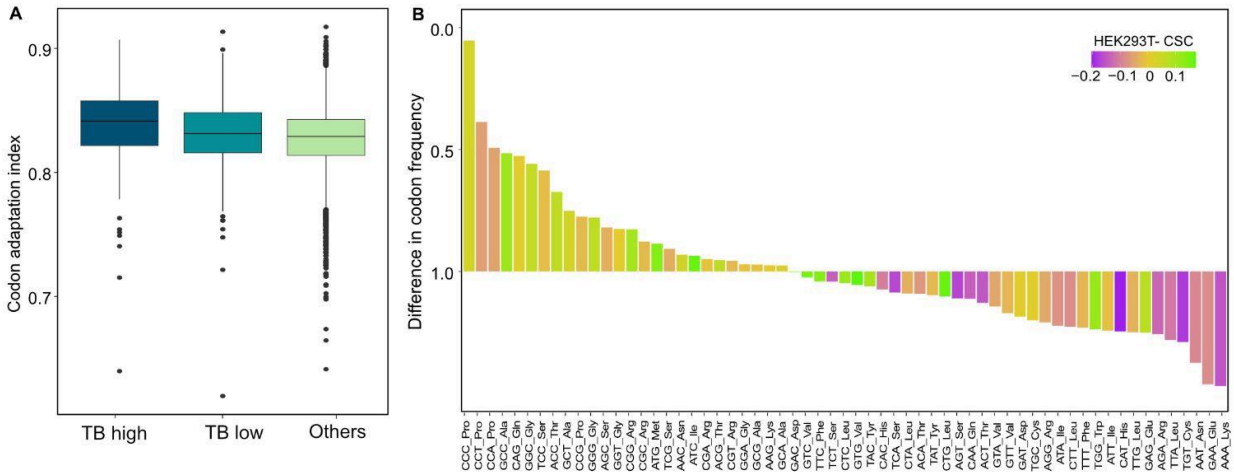

Sup. Fig 4: A. Box plot showing the codon adaptation index of human genes belonging to three categories. (TB high; n=250, TB mid; n= 250; Others; n= 7934). **B.** Bar plot showing the difference in codon frequency between “low” and non-buffered genes The bars are colored according to the codon stabilization coefficient obtained from [29]. n refers to the number of genes

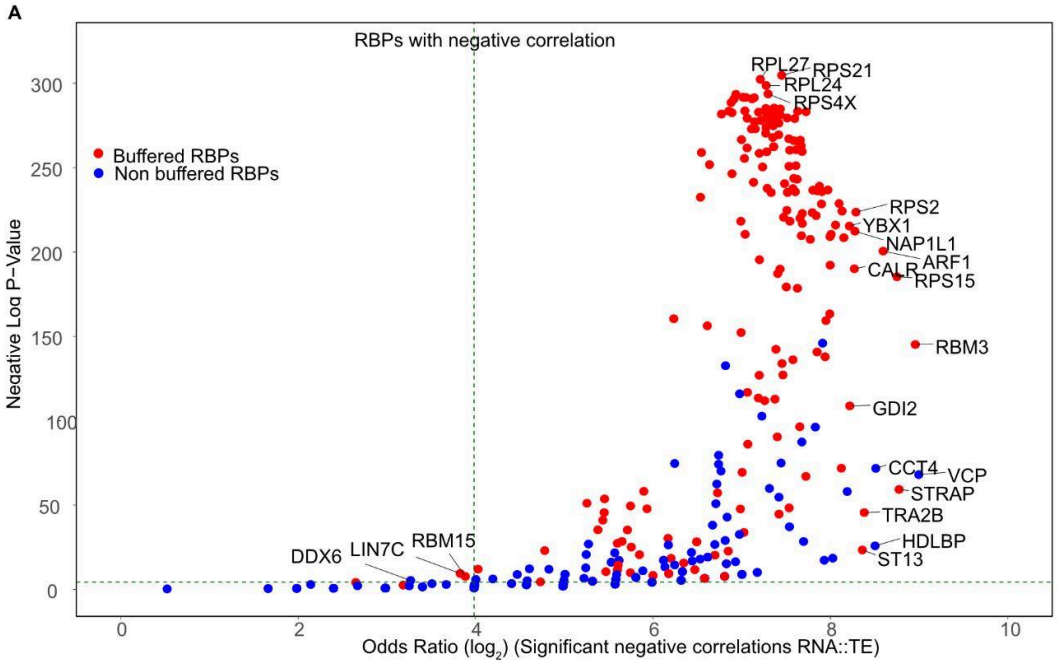
A
RBPs with negative correlation
Buffered RBPs
Non buffered RBPs
Negative Log P−Value
Odds Ratio (log2) (Significant negative correlations RNA::TE)
RPL27
RPS21
RPL24
RPS4X
RPS2
YBX1
NAP1L1
ARF1
CALR
RPS15
RBM3
GDI2
CCT4
VCP
STRAP
TRA2B
HDLBP
ST13
DDX6
LIN7C
RBM15

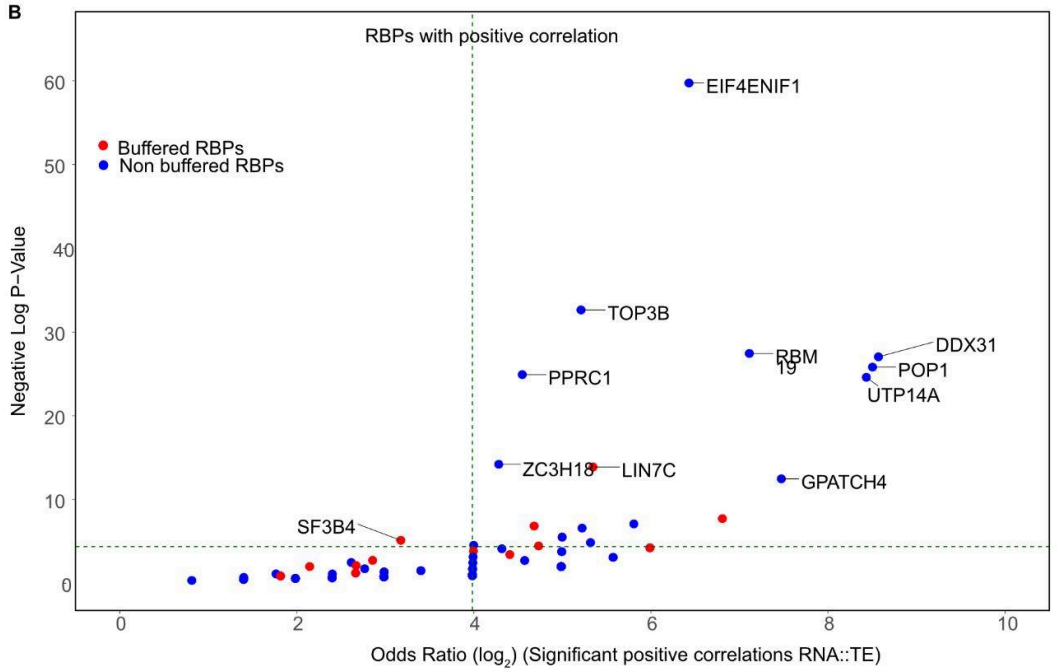
B
RBPs with positive correlation
Buffered RBPs
Non buffered RBPs
Negative Log P−Value
Odds Ratio (log2) (Significant positive correlations RNA::TE)
EIF4ENIF1
TOP3B
RBM 19
DDX31
POP1
UTP14A
PPRC1
ZC3H18
LIN7C
GPATCH4
SF3B4

Sup. Fig 5: A scatter plot of odds ratio $\log_2$ of number of significant correlations (RNA abundance of RBPs ::TE of genes) and the p value from fisher test. The vertical dashed line represents the threshold odds ratio, above which RBPs exhibit a higher number of significant correlations with buffered genes. P values were corrected using Bonferroni procedure and the horizontal dashed line represents the adjusted p value cutoff.

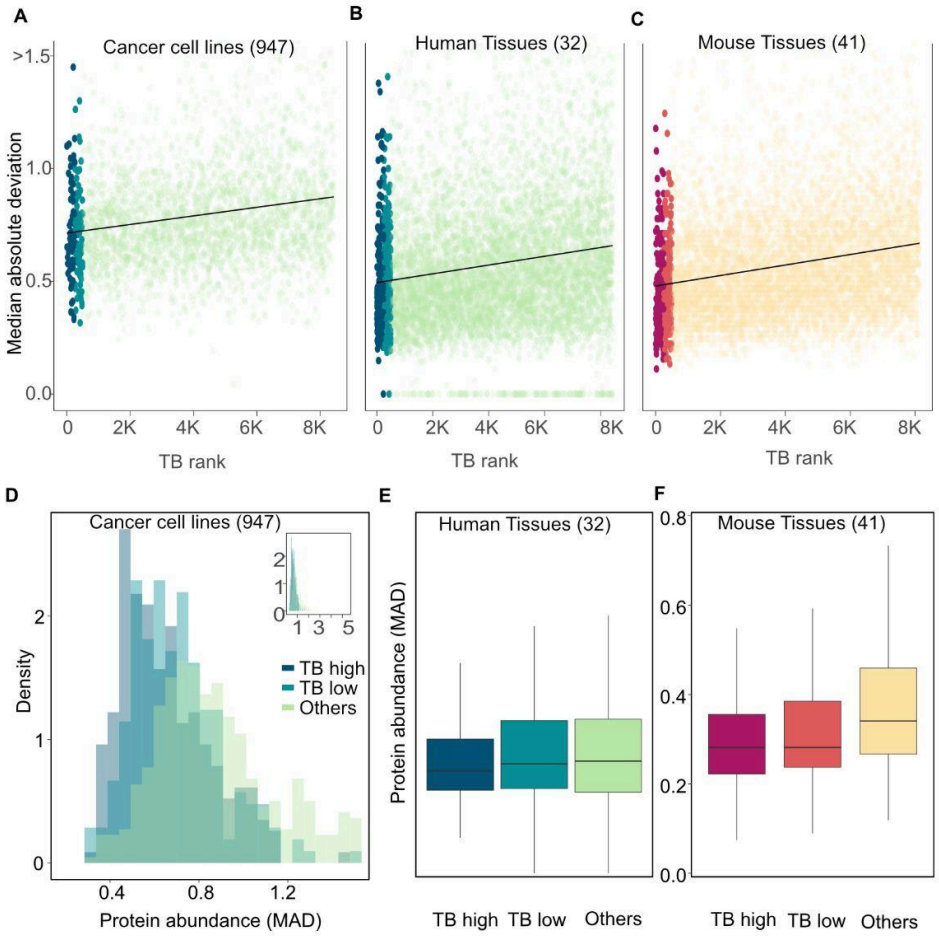

Sup. Fig 6: Scatter plot showing the relation between rank and median absolute deviation of proteins in A. Cancer cell line **B.** Human tissues C. Mouse tissue. Linear regression trend line is shown in black. Boxplot showing the MAD of protein abundance of genes with non-buffered genes selected with similar mRNA MAD as the buffered genes from **D.** human cancer cell lines from [34] (TB high; n=221, TB mid; n= 202; Others; n= 423) **E.** human primary tissue from [35] (TB high; n=233, TB mid; n= 227; Others; n= 460) and **F.** mouse tissues from [36] (TB high; n=189 TB mid; n= 199; Others; n=388). Genes selected in the "Others" category were derived by a matching procedure (Methods). n refers to the number of genes

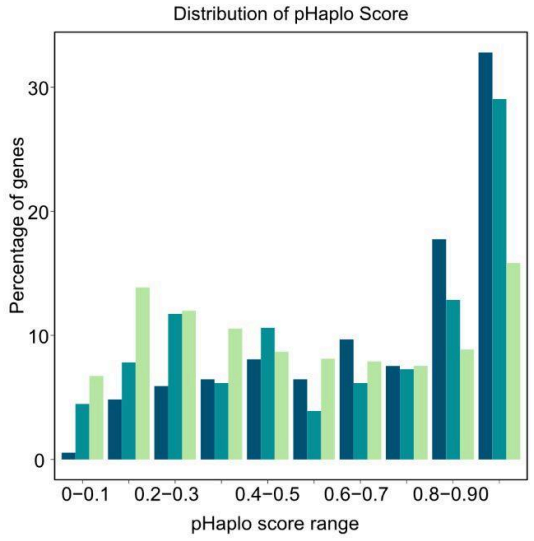

Sup. Fig 7: Collins et al. 2022 predicts the haplosensitivity for all autosomal genes referred to as pHaplo score. Bar plot shows a higher median Haplo score than the non-buffered set (TB high; n=187, TB mid; n= 173; Others; n= 11128). n refers to the number of genes

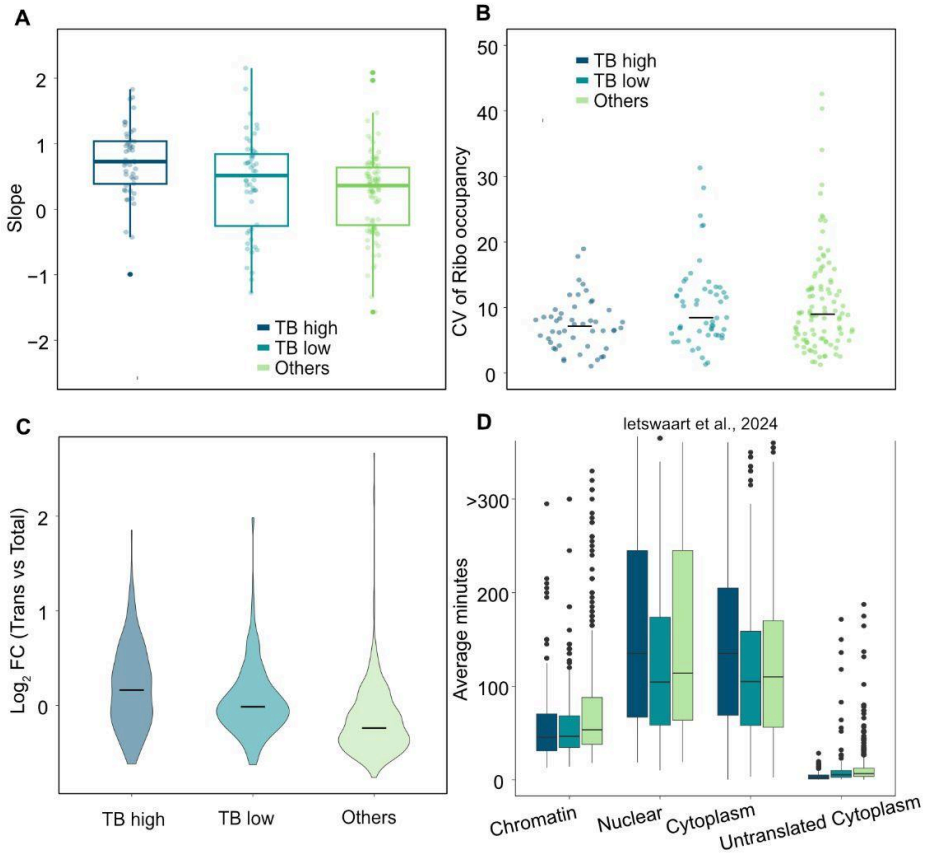

Sup. Fig 8: A. Box plot showing the slope between translational RNA and total RNA for the buffered and non-buffered gene set (TB high; n=48, TB low; n= 42; Others; n=100). non-buffered genes were selected based on their similarity with CV of buffered genes using a

matching approach (See Methods) **B.** Sina plot showing the CV of ribosome occupancy levels of the three gene sets from the ribosome profiling experiment carried out in parallel to the RNA-seq of total and translating RNA. Particularly, non-buffered genes were selected based on their similarity with CV of buffered genes using a matching approach (See Methods) (high; n=48, low; n= 52; others; n=100). **C.** Violin plot showing the $\log_2$ fold change between the translational mRNA and total mRNA of genes in three categories (TB high; n=250, TB low; n= 250; Others; n=500). non-buffered genes were selected based on their similarity with expression (cpm values) of buffered genes using a matching approach (See Methods) **D.** Box plot showing the half life measurements of the three categories of gene sets in different compartments including the chromatin, nucleus, untranslated cytoplasm and the cytoplasm wherein the genes in the control set is selected to match the half life of the transcripts in “TB high” and TB low” categories (TB high; n=249, TB low; n= 246; Others; n=495). The half life measurements of mRNA were obtained from [38]. n refers to the number of genes

Supplementary text:

To validate translational buffering, we attempted to generate a series of knockdowns of buffered genes using the MultiCas12a approach described in [65]. Briefly, we synthesized a three 10-plex cRNA array targeting 8 buffered and 2 non-buffered genes as double stranded gene fragments (Twist Biosciences). The arrays differed in the gRNA efficiency of their target. A fourth crRNA array targeted the intergenic region to be used as a negative control. Overall, four 10-plex crRNA were cloned in pCH67 into the Bsmb1 cloning site (Addgene, 217667) using NEBuilder HiFi DNA Assembly Master Mix (NEB, E2621). Lentivirus was generated with the cloned pCH67 or pCH45 (multiAsCas12a-KRAB, Agdgene, 217330) along with psPAX2 (Addgene, 12260)and pMD2.G (Addgene ,2259) using lipofectamine 3000 (Invitrogen) as per manufacturer's protocol.The lentivirus was used to infect HEK293T cells followed by selection using puromycin. Following selection, BFP positive cells were sorted using FACS to select for cells that express MultiCas12a. HEK293T cells were then continued to grow for 24 hours followed by plating in 150 cm2 plates to perform ribosome profiling, with matched total and translating RNA sequencing. As the knockdown efficiency was low with this approach, we leveraged natural variation in gene expression across replicates in this data to assess the mechanism of translational buffering.

Acknowledgements:

This work was supported in part by the National Institutes of Health (R35GM150667; HD110096), and the Welch Foundation [F-2027-20230405] (C.C.). All of the original text in this paper was written by the authors. We thank Dr. Vighnesh Ghatpande for valuable suggestions. We used two LLMs; ChatGPT and UT Spark for the following purposes: 1. to improve clarity and grammar of the text and 2. To generate code for data visualization and statistical analysis which was subsequently reviewed, edited and tested before being implemented for final analysis.

Author Contributions:

S.R, and C.C. wrote the manuscript. L.P developed the LGBM model, S.R. and A.L. carried out all other analyses; S.R. carried out all experiments. C.C. provided study oversight, conceptualized the study and acquired funding. All authors approved the final manuscript.

Data availability:

Sequencing data and ribo files for the sequencing experiments is available on GEO accession: GSE297442.

Code Availability

The code used in the study is available at
https://github.com/CenikLab/Translational-buffering/tree/Translational-Buffering

References

1. Raj A, van Oudenaarden A. Nature, nurture, or chance: stochastic gene expression and its consequences. Cell. 2008;135:216–26.

2. Gandhi SJ, Zenklusen D, Lionnet T, Singer RH. Transcription of functionally related constitutive genes is not coordinated. Nat Struct Mol Biol. 2011;18:27–34.

3. Elowitz MB, Levine AJ, Siggia ED, Swain PS. Stochastic gene expression in a single cell. Science. 2002;297:1183–6.

4. Dephoure N, Hwang S, O'Sullivan C, Dodgson SE, Gygi SP, Amon A, et al. Quantitative proteomic analysis reveals posttranslational responses to aneuploidy in yeast. Elife. 2014;3:e03023.

5. Zhang B, Wang J, Wang X, Zhu J, Liu Q, Shi Z, et al. Proteogenomic characterization of human colon and rectal cancer. Nature. 2014;513:382–7.

6. Cenik C, Cenik ES, Byeon GW, Grubert F, Candille SI, Spacek D, et al. Integrative analysis of RNA, translation, and protein levels reveals distinct regulatory variation across humans. Genome Res. 2015;25:1610–21.

7. Lundberg E, Fagerberg L, Klevebring D, Matic I, Geiger T, Cox J, et al. Defining the transcriptome and proteome in three functionally different human cell lines. Mol Syst Biol. 2010;6:450.

8. Stingele S, Stoehr G, Peplowska K, Cox J, Mann M, Storchova Z. Global analysis of genome, transcriptome and proteome reveals the response to aneuploidy in human cells. Mol Syst Biol. 2012;8:608.

9. Kustatscher G, Grabowski P, Rappsilber J. Pervasive coexpression of spatially proximal genes is buffered at the protein level. Mol Syst Biol. 2017;13:937.

10. Liu Y, Beyer A, Aebersold R. On the Dependency of Cellular Protein Levels on mRNA Abundance. Cell. 2016;165:535–50.

11. Kusnadi EP, Timpone C, Topisirovic I, Larsson O, Furic L. Regulation of gene expression via translational buffering. Biochim Biophys Acta Mol Cell Res. 2022;1869:119140.

12. Muenzner J, Trébulle P, Agostini F, Zauber H, Messner CB, Steger M, et al. Natural proteome diversity links aneuploidy tolerance to protein turnover. Nature. 2024;630:149–57.

13. Teyssonnière EM, Trébulle P, Muenzner J, Loegler V, Ludwig D, Amari F, et al. Species-wide quantitative transcriptomes and proteomes reveal distinct genetic control of gene expression variation in yeast. Proc Natl Acad Sci U S A. 2024;121:e2319211121.

14. Gonçalves E, Fragoulis A, Garcia-Alonso L, Cramer T, Saez-Rodriguez J, Beltrao P. Widespread post-transcriptional attenuation of genomic copy-number variation in cancer. Cell Syst. 2017;5:386–98.e4.

15. Buccitelli C, Selbach M. mRNAs, proteins and the emerging principles of gene expression control. Nat Rev Genet. 2020;21:630–44.

16. Artieri CG, Fraser HB. Evolution at two levels of gene expression in yeast. Genome Res. 2014;24:411–21.

17. McManus CJ, May GE, Spealman P, Shteyman A. Ribosome profiling reveals post-transcriptional buffering of divergent gene expression in yeast. Genome Res. 2014;24:422–30.

18. Teyssonniere EM, Shichino Y, Mito M, Friedrich A, Iwasaki S, Schacherer J. Translation variation across genetic backgrounds reveals a post-transcriptional buffering signature in yeast. Nucleic Acids Res. 2024;52:2434–45.

19. Blevins WR, Tavella T, Moro SG, Blasco-Moreno B, Closa-Mosquera A, Díez J, et al. Extensive post-transcriptional buffering of gene expression in the response to severe oxidative stress in baker's yeast. Sci Rep. 2019;9:11005.

20. Lorent J, Kusnadi EP, van Hoef V, Rebello RJ, Leibovitch M, Ristau J, et al. Translational offsetting as a mode of estrogen receptor α-dependent regulation of gene expression. EMBO J. 2019;38:e101323.

21. Wang Z-Y, Leushkin E, Liechti A, Ovchinnikova S, Mößinger K, Brüning T, et al. Transcriptome and translatome co-evolution in mammals. Nature. 2020;588:642–7.

22. Ozadam H, Tonn T, Han CM, Segura A, Hoskins I, Rao S, et al. Single-cell quantification of ribosome occupancy in early mouse development. Nature. 2023;618:1057–64.

23. Liu Y, Rao S, Hoskins I, Geng M, Zhao Q, Chacko J, et al. Translation efficiency covariation identifies conserved coordination patterns across cell types. Nat Biotechnol. 2025;1–13.

24. Larsson O, Sonenberg N, Nadon R. Identification of differential translation in genome wide studies. Proc Natl Acad Sci U S A. 2010;107:21487–92.

25. Albert FW, Muzzey D, Weissman JS, Kruglyak L. Genetic influences on translation in yeast. PLoS Genet. 2014;10:e1004692.

26. Sharp PM, Li WH. The codon Adaptation Index--a measure of directional synonymous codon usage bias, and its potential applications. Nucleic Acids Res. 1987;15:1281–95.

27. Lyons EF, Devanneaux LC, Muller RY, Freitas AV, Meacham ZA, McSharry MV, et al. Translation elongation as a rate limiting step of protein production . Molecular Biology. bioRxiv; 2023. Available from: https://www.biorxiv.org/content/10.1101/2023.11.27.568910v2.full.pdf

28. Barrington CL, Galindo G, Koch AL, Horton ER, Morrison EJ, Tisa S, et al. Synonymous codon usage regulates translation initiation. Cell Rep. 2023;42:113413.

29. Wu Q, Medina SG, Kushawah G, DeVore ML, Castellano LA, Hand JM, et al. Translation affects mRNA stability in a codon-dependent manner in human cells. Elife. 2019;8. Available from: http://dx.doi.org/10.7554/eLife.45396

30. Zheng D, Persyn L, Wang J, Liu Y, Ulloa-Montoya F, Cenik C, et al. Predicting the translation efficiency of messenger RNA in mammalian cells. Nat Biotechnol. 2025;1–14.

31. Agarwal V, Kelley DR. The genetic and biochemical determinants of mRNA degradation rates in mammals. Genome Biol. 2022;23:245.

32. Hentze MW, Castello A, Schwarzl T, Preiss T. A brave new world of RNA-binding proteins. Nat Rev Mol Cell Biol. 2018;19:327–41.

33. Qi K, Cenik C. Topological and functional characterization of human translation efficiency covariation network. Bioinformatics. 2025; Available from: http://dx.doi.org/10.1093/bioinformatics/btaf583/8300552

34. Gonçalves E, Poulos RC, Cai Z, Barthorpe S, Manda SS, Lucas N, et al. Pan-cancer proteomic map of 949 human cell lines. Cancer Cell. 2022;40:835–49.e8.

35. Jiang L, Wang M, Lin S, Jian R, Li X, Chan J, et al. A Quantitative Proteome Map of the Human Body. Cell. 2020;183:269–83.e19.

36. Giansanti P, Samaras P, Bian Y, Meng C, Coluccio A, Frejno M, et al. Mass spectrometry-based draft of the mouse proteome. Nat Methods. 2022;19:803–11.

37. Collins RL, Glessner JT, Porcu E, Lepamets M, Brandon R, Lauricella C, et al. A cross-disorder dosage sensitivity map of the human genome. Cell. 2022;185:3041–55.e25.

38. Ietswaart R, Smalec BM, Xu A, Choquet K, McShane E, Jowhar ZM, et al. Genome-wide quantification of RNA flow across subcellular compartments reveals determinants of the mammalian transcript life cycle. Mol Cell. 2024;84:2765–84.e16.

39. Wiggan O ’neil, Stasevich TJ. Single molecule imaging of the central dogma reveals myosin-2A gene expression is regulated by contextual translational buffering. bioRxiv : the preprint server for biology. 2024. Available from: https://pubmed.ncbi.nlm.nih.gov/38370738/

40. Bader DM, Wilkening S, Lin G, Tekkedil MM, Dietrich K, Steinmetz LM, et al. Negative feedback buffers effects of regulatory variants. Mol Syst Biol. 2015;11:785.

41. Chothani S, Adami E, Ouyang JF, Viswanathan S, Hubner N, Cook SA, et al. DeltaTE: Detection of translationally regulated genes by integrative analysis of Ribo-seq and RNA-seq data. Curr Protoc Mol Biol. 2019;129:e108.

42. Zhong Y, Karaletsos T, Drewe P, Sreedharan VT, Kuo D, Singh K, et al. RiboDiff: detecting changes of mRNA translation efficiency from ribosome footprints. Bioinformatics. 2017;33:139–41.

43. Oertlin C, Lorent J, Murie C, Furic L, Topisirovic I, Larsson O. Generally applicable transcriptome-wide analysis of translation using anota2seq. Nucleic Acids Res. 2019;47:e70.

44. Weidemann DE, Holehouse J, Singh A, Grima R, Hauf S. The minimal intrinsic stochasticity of constitutively expressed eukaryotic genes is sub-Poissonian. Sci Adv. 2023;9:eadh5138.

45. Philippe L, van den Elzen AMG, Watson MJ, Thoreen CC. Global analysis of LARP1 translation targets reveals tunable and dynamic features of 5’ TOP motifs. Proc Natl Acad Sci U S A. 2020;117:5319–28.

46. Gentilella A, Morón-Duran FD, Fuentes P, Zweig-Rocha G, Riaño-Canalias F, Pelletier J, et al. Autogenous Control of 5′TOP mRNA Stability by 40S Ribosomes. Mol Cell. 2017;67:55–70.e4.

47. Saba JA, Huang Z, Schole KL, Ye X, Bhatt SD, Li Y, et al. LARP1 binds ribosomes and TOP

mRNAs in repressed complexes. EMBO J. 2024;43:6555–72.

48. Jüschke C, Dohnal I, Pichler P, Harzer H, Swart R, Ammerer G, et al. Transcriptome and proteome quantification of a tumor model provides novel insights into post-transcriptional gene regulation. Genome Biol. 2013;14:r133.

49. Bottorff TA, Park H, Geballe AP, Subramaniam AR. Translational buffering by ribosome stalling in upstream open reading frames. PLoS Genet. 2022;18:e1010460.

50. Surya A, Bolton BM, Rothe R, Mejia-Trujillo R, Leonita A, Zhao Q, et al. Differential impacts of ribosomal protein haploinsufficiency on mitochondrial function. J Cell Biol . 2025 [cited 2025 May 13];224. Available from: http://dx.doi.org/10.1083/jcb.202404084

51. Palarea-Albaladejo J, Martín-Fernández JA. zCompositions — R package for multivariate imputation of left-censored data under a compositional approach. Chemometr Intell Lab Syst. 2015;143:85–96.

52. Wu T, Hu E, Xu S, Chen M, Guo P, Dai Z, et al. clusterProfiler 4.0: A universal enrichment tool for interpreting omics data. Innovation (Camb). 2021;2:100141.

53. Quinlan AR, Hall IM. BEDTools: a flexible suite of utilities for comparing genomic features. Bioinformatics. 2010;26:841–2.

54. Pagès H, Aboyoun P, Gentleman R, DebRoy S. Biostrings: Efficient manipulation of biological strings. R package version. 2019;2:10–18129.

55. Ho DE, Imai K, King G, Stuart EA. Matching as nonparametric preprocessing for reducing model dependence in parametric causal inference. Polit Anal. 2007;15:199–236.

56. Codon Usage Bias Analysis [R package cubar version 1.1.0]. 2024 [cited 2025 Apr 14]; Available from: https://CRAN.R-project.org/package=cubar

57. Gamble CE, Brule CE, Dean KM, Fields S, Grayhack EJ. Adjacent codons act in concert to modulate translation efficiency in yeast. Cell. 2016;166:679–90.

58. Ke G, Meng Q, Finley T, Wang T, Chen W, Ma W, et al. LightGBM: A highly efficient gradient boosting decision tree. Neural Inf Process Syst. 2017;3146–54.

59. Karczewski KJ, Francioli LC, Tiao G, Cummings BB, Alföldi J, Wang Q, et al. The mutational constraint spectrum quantified from variation in 141,456 humans. Nature. 2020;581:434–43.

60. Robinson MD, Oshlack A. A scaling normalization method for differential expression analysis of RNA-seq data. Genome Biol. 2010;11:R25.

61. Robinson MD, McCarthy DJ, Smyth GK. edgeR: a Bioconductor package for differential expression analysis of digital gene expression data. Bioinformatics. 2010;26:139–40.

62. Rao S, Hoskins I, Tonn T, Garcia PD, Ozadam H, Sarinay Cenik E, et al. Genes with 5' terminal oligopyrimidine tracts preferentially escape global suppression of translation by the SARS-CoV-2 Nsp1 protein. RNA. 2021;27:1025–45.

63. Ozadam H, Geng M, Cenik C. RiboFlow, RiboR and RiboPy: an ecosystem for analyzing ribosome profiling data at read length resolution. Bioinformatics. 2020;36:2929–31.

64. Chacko J, Ozadam H, Cenik C. RiboGraph: an interactive visualization system for ribosome profiling data at read length resolution. Bioinformatics. 2024;40:btae369.

65. Hsiung CC-S, Wilson CM, Sambold NA, Dai R, Chen Q, Teyssier N, et al. Engineered CRISPR-Cas12a for higher-order combinatorial chromatin perturbations. Nat Biotechnol. 2025;43:369–83.